

1 **South Asian summer monsoon enhanced by the uplift of Iranian Plateau in**
2 **Middle Miocene**

a mis en forme : Couleur de police : Automatique

3 Meng Zuo^{1,2}, Yong Sun³, Yan Zhao^{3*}, Gilles Ramstein⁴, Lin Ding³, Tianjun Zhou¹

4 *1 LASG, Institute of Atmospheric Physics, Chinese Academy of Sciences, Beijing, China*

a mis en forme : Couleur de police : Automatique

5 *2, State Key Laboratory of Severe Weather and Institute of Tibetan Plateau Meteorology,*
6 *Chinese Academy of Meteorological Sciences, Beijing, China*

a supprimé:

a mis en forme : Couleur de police : Automatique

7 *3 Key Laboratory of Continental Collision and Plateau Uplift, Institute of Tibetan Plateau*
8 *Research, and Center for Excellence in Tibetan Plateau Earth Sciences, Chinese Academy of*
9 *Sciences, Beijing 100101, China*

10 *4 Laboratoire des Sciences du Climat et de l'environnement, CNRS-CEA-UVSQ, 91191 Gif-*
11 *sur-Yvette, France*

12
13 **Correspondence to [Yan Zhao](mailto:yan.zhao@itpcas.ac.cn); yan.zhao@itpcas.ac.cn**

a supprimé: yan zhao:

a mis en forme : Couleur de police : Automatique

17 **ABSTRACT**

18 The South Asian summer monsoon (SASM) significantly intensified during the Middle
19 Miocene (17-12 Ma), but the driver of this change remains an open question. The uplift of the
20 Himalaya (HM) and the Iranian Plateau (IP), and global CO₂ variation are prominent factors
21 among suggested drivers. Particularly, the impact of high CO₂ levels on the Miocene SASM
22 has been little studied, despite the wide range of reconstructed CO₂ values around this period.
23 Here we investigate their effects on the SASM using the fully coupled Ocean-Atmosphere
24 Global Climate Model CESM1.2 through a series of 12 sensitivity experiments. Our
25 simulations show that the IP uplift plays a dominant role in the intensification of the SASM,
26 mainly in the region around northwestern India. The effect of the HM uplift is confined to the
27 range of the HM and its vicinity, producing orographic precipitation change. The topography
28 forcing overall out-competes CO₂ variation in driving the intensification of the SASM. In the
29 case of extremely strong CO₂ variation, the effects of these two factors are comparable in the
30 core SASM region, while in the western region, the topographic forcing is still the dominant
31 driver. We propose a thermodynamical process linking the uplift of the IP and the enhanced
32 SASM through the release of latent heat. Compared with reconstructions, the simulated
33 response of SASM to the IP uplift is in good agreement with observed precipitation and wind
34 fields, while the effects of the HM uplift and CO₂ variation are inadequate to interpret the proxies.

35
36 **Keywords:** South Asian summer monsoon, Middle Miocene, topographic change, CO₂
37 variation, thermal heating effect

- a supprimé: to
- a mis en forme : Couleur de police : Automatique
- a mis en forme : Couleur de police : Automatique
- a mis en forme : Couleur de police : Automatique
- a mis en forme : Couleur de police : Automatique
- a supprimé: is
- a mis en forme : Couleur de police : Automatique
- a supprimé: a large
- a mis en forme : Couleur de police : Automatique
- a mis en forme : Couleur de police : Automatique

- a supprimé: the
- a mis en forme : Couleur de police : Automatique
- a mis en forme : Couleur de police : Automatique
- a supprimé: A
- a supprimé: is proposed to link
- a mis en forme : Couleur de police : Automatique
- a mis en forme : Couleur de police : Automatique
- a mis en forme : Couleur de police : Automatique
- a mis en forme : Couleur de police : Automatique
- a supprimé: heating release.
- a mis en forme : Couleur de police : Automatique
- a mis en forme : Couleur de police : Automatique
- a mis en forme : Couleur de police : Automatique

46 **1. Introduction**

47 The Middle Miocene (17-12 Ma) was a period characterized by major climatic, tectonic,
48 CO₂ and environmental changes (Steinthorsdottir et al., 2021). Increasing evidence indicates
49 that the South Asian summer monsoon (SASM) was remarkably intensified in the Middle
50 Miocene (Clift et al., 2008; Clift and Webb, 2019; Gupta et al., 2015; Bialik et al., 2020; Bhatia
51 et al., 2021; Vogeli et al., 2017) although its inception was no later than the Early Miocene (Ali
52 et al. 2021, Licht, 2014; Farnsworth et al., 2019). However, the driving factor of its evolution
53 remains an issue of great debate. Besides the effect of geographic change (Ramstein et al., 1997;
54 Fluteau et al., 1999; Farnsworth et al., 2019; Thomason et al., 2021; Tardif et al., 2020, 2023;
55 Sarr et al., 2022), the growth of the Himalaya (HM)-Tibetan Plateau (TP; HM-TP) has
56 traditionally been called for the SASM development (Cliff et al., 2008; Clift and Webb, 2019;
57 Manabe and Terpstra, 1974; Kutzbach et al., 1989; Prell and Kutzbach, 1992; Ramstein et al.,
58 1997; An et al., 2001; Kitoh, 2002; Chakraborty et al., 2006; Wu et al., 2012; Tada et al., 2016;
59 Tarif et al., 2020, 2023). The HM, which has long been regarded as the “southern TP” (Spicer,
60 2017), receives particular attention (Boos and Kuang, 2010; Wu et al., 2012; Zhang et al., 2015).
61 Recent geological evidence (Liu et al., 2016; Ding et al., 2017, 2022) suggests that, in contrast
62 to previous studies, the HM had risen to a height of 2.3 ± 0.9 km by the earliest Miocene,
63 reaching approximately 4 km by 19 Ma. From 15 Ma onwards, the HM projected significantly
64 above the average elevation of the plateau that had already attained its modern height before
65 the Miocene (Wang et al., 2014). The coincidence of the ongoing HM uplift above the TP since
66 15 Ma and the intensification of SASM appears to support the hypothesis that the evolution of
67 the SASM is predominantly driven by the formation of HM-TP.

68 However, this traditional view is challenged by many modeling studies that emphasize the
69 importance of peripheral mountain ranges (Chakraborty et al., 2006; Tardif et al., 2020, 2023;
70 Sarr et al., 2022; Liu et al., 2017; Tang et al., 2013; Chen et al., 2014; Acosta and Huber, 2020).
71 Notably, the Iranian Plateau (IP), which also underwent uplift during the same period as the
72 Miocene SASM enhancement around 15-12 Ma, is considered a critical factor (McQuarrie et
73 al., 2003; Mouthereau, 2011; Ballato et al., 2017; Bialik et al., 2020), although the evolution
74 history of the IP’s build-up remains hotly debated (Agard et al., 2011; McQuarrie et al., 2003;
75 Mouthereau, 2011; Ballato et al., 2017). Nevertheless, most studies suggest a Miocene age for
76 the uplift of most landforms. Geological evidence indicates that in the northern sectors of the
77 IP, the uplift likely occurred between 16.5-10.7 Ma (Ballato et al., 2017), particularly
78 accelerated after 12.4 Ma (Mouthereau, 2011) while in regions bordering the IP to the south,

a supprimé: evidences indique

a mis en forme : Couleur de police : Automatique

a supprimé: Zhuang et al., 2017;

a mis en forme : Couleur de police : Automatique

a mis en forme : Couleur de police : Automatique

a mis en forme : Couleur de police : Automatique

a supprimé: Zhuang et al., 2017;

a mis en forme : Couleur de police : Automatique

a mis en forme : Couleur de police : Automatique

a mis en forme : Couleur de police : Automatique

a mis en forme : Couleur de police : Automatique

a mis en forme : Couleur de police : Automatique

a mis en forme : Couleur de police : Automatique

a mis en forme : Couleur de police : Automatique

a supprimé: ¶

a mis en forme : Couleur de police : Automatique

a supprimé: evidences

a mis en forme : Couleur de police : Automatique

a supprimé: suggest

a mis en forme : Couleur de police : Automatique

a supprimé: . This elevation was notably higher than the TP, which...

a supprimé: reached

a mis en forme : Couleur de police : Automatique

a supprimé: rapid

a supprimé: which

a mis en forme : Couleur de police : Automatique

a mis en forme : Couleur de police : Automatique

a supprimé: experienced

a mis en forme : Couleur de police : Automatique

a supprimé: regarded as

a mis en forme : Couleur de police : Automatique

a mis en forme : Couleur de police : Automatique

a mis en forme : Couleur de police : Automatique

a mis en forme : Couleur de police : Automatique

a mis en forme : Couleur de police : Automatique

a mis en forme : Couleur de police : Automatique

a mis en forme : Couleur de police : Automatique

a mis en forme : Couleur de police : Automatique

a mis en forme : Couleur de police : Automatique

a supprimé:). Therefore, the contribution of the IP and HM uplift to intensified SASM during the Middle Miocene remains

94 uplift occurred between 15 and 5 Ma (Mouthereau, 2011). The Zagros orogen, a significant part
 95 of the IP, developed in three distinct pulses within the last ~20 Ma (Agard et al., 2011;
 96 Mouthereau, 2011). Therefore, there exists significant uncertainty regarding the growth of the
 97 IP. The respective contributions of the IP and HM uplift to intensified SASM during the Middle
 98 Miocene remain unclear.

99 Various mechanisms were proposed to explain the linkage between the uplift of the IP and
 100 HM and the intensification of SASM rainfall. These include the mechanical blocking effect
 101 (Tang et al., 2013), topographic thermal forcing (Chen et al., 2014; Wu et al., 2012; Liu et al.,
 102 2017), and the role of gatekeeper to insulate the pool of high-enthalpy air in northern India from
 103 westerly advection of cool and dry air (Acosta and Huber, 2020). However, most of these
 104 modeling studies have examined the effects of IP and HM uplift using Atmospheric General
 105 Circulation Model (AGCM) with modern geographies (Liu et al., 2017; Zhang et al., 2015;
 106 Tang et al., 2013; Acosta and Huber, 2020), potentially overlooking two key factors: 1) the
 107 neglect of air-sea interaction processes (Kitoh, 2002; Su et al., 2018); 2) the risk of
 108 misinterpreting past changes due to the critical role of land-sea distribution in shaping the
 109 paleoclimate features (Tardif et al., 2023; Ramstein et al., 1997). Therefore, we opt to use a
 110 fully coupled Ocean-Atmosphere Global Climate Model (OAGCM) to revisit the response of
 111 the SASM to the IP and HM uplift under Miocene boundary conditions despite requiring
 112 additional computational resources.

113 The SASM is sensitive to changes in CO₂ concentration (Thomson et al., 2021). The effect
 114 of CO₂ variation is overall estimated to be less than that of geography and/or topography
 115 (Farnsworth et al., 2019; Thomson et al., 2021; Tardif et al., 2023), however, during the mid-
 116 to-late Miocene, its contribution to rainfall change is comparable to that of orographic uplift
 117 even when the CO₂ is set from 560 ppm to 280 ppm (Thomson et al., 2021). Proxy records
 118 indicate that the early to middle Miocene was a warming period, which is known as the Middle
 119 Miocene Climatic Optimum (~17-14 Ma), followed by a late Miocene cooling (Steinthorsdottir
 120 et al., 2021). There is large uncertainty in estimated CO₂ variation in the Middle Miocene, with
 121 a wide range of reconstructed values from ~180 ppmv to ~600 ppmv (Foster and Rohling,
 122 2013; Pagani et al., 1999; Steinthorsdottir et al., 2021; The CenCO₂PIP, 2023, and reference
 123 herein), even to more than 1000 ppmv (Rae et al., 2021) during the Middle Miocene Climatic
 124 Optimum. Nevertheless, according to general concept, the atmospheric CO₂ concentration
 125 peaked around 15 Ma and then declined (The CenCO₂PIP, 2023). Therefore, it is necessary to
 126 re-examine the effect of CO₂ forcing on SASM rainfall based on the possible range of CO₂
 127 variation.

- a supprimé: , including
- a mis en forme (... [1])
- a supprimé: based on
- a mis en forme : Couleur de police : Automatique
- a supprimé: general circulation model
- a mis en forme : Couleur de police : Automatique
- a supprimé: which may result in
- a mis en forme : Couleur de police : Automatique
- a supprimé: issues
- a mis en forme : Couleur de police : Automatique
- a supprimé: neglecting
- a mis en forme (... [2])
- a supprimé: process
- a mis en forme (... [3])
- a supprimé: ; Wang et al., 2019); 2) a misleading interpretation for
- a mis en forme : Couleur de police : Automatique
- a supprimé: it is worthy
- a mis en forme : Couleur de police : Automatique
- a supprimé: with a fully coupled Ocean-Atmosphere Global Climate Model (OAGCM) and investigate the underlying physical processes, which have been rarely studied before (Sarr et al., 2022; Tardif et al., 2023).
- a mis en forme : Couleur de police : Automatique
- a supprimé: Thomason...homson et al., 2021). The effect of (... [4])
- a mis en forme : Couleur de police : Automatique
- a supprimé: Thomason...homson et al., 2021; Tardif et al., 2023), however, during the mid-to-late Miocene, its contribution to rainfall change is comparable to that of orographic uplift even when the pCO₂...O₂ is set from 560 ppm to 280 ppm to 560 ppm ... The (... [5])
- a mis en forme (... [6])
- a supprimé: 2021b
- a mis en forme (... [7])
- a supprimé: pCO₂
- a mis en forme (... [8])
- a supprimé: pCO₂
- a mis en forme : Couleur de police : Automatique
- a supprimé: pCO₂
- a mis en forme : Couleur de police : Automatique
- a supprimé:
- a mis en forme : Couleur de police : Automatique

175 In this study, we utilize a fully coupled OAGCM to explore the impact of IP and HM uplift
 176 and the CO₂ variation on the SASM. Considering that the uplift of HM and IP predominantly
 177 occurred after 15 Ma, roughly coinciding with pronounced CO₂ variations during 17-14 Ma,
 178 we conduct two sets of sensitivity experiments based on Middle Miocene geography. The
 179 topographic sensitivity experiments are placed into the context of the current understanding of
 180 the regional tectonic and geographic settings while a set of CO₂ sensitivity experiments ranging
 181 from 280 to 1000 ppmv is performed. The model configuration, Middle Miocene boundary
 182 condition and experimental design are described in Section 2. In Section 3, we show the SASM
 183 response to IP and HM uplift, and the effect of CO₂ forcing. The mechanisms responsible for
 184 the monsoonal precipitation change are examined in Section 4. The implication of our results
 185 to the evolution of the SASM in the Middle Miocene is discussed in Section 5 before giving
 186 conclusions in Section 6.

a supprimé: is employed
 a mis en forme : Couleur de police : Automatique
 a mis en forme : Couleur de police : Automatique

a mis en forme : Couleur de police : Automatique

a supprimé: . A
 a mis en forme : Couleur de police : Automatique
 a supprimé: with a range of values
 a mis en forme : Couleur de police : Automatique
 a supprimé: based on the Middle Miocene geography
 a mis en forme : Couleur de police : Automatique

a mis en forme : Couleur de police : Automatique

187 2. Data and Methods

188 2.1. Climate model

189 The model used in this study is the Community Earth System Model (CESM), Version
 190 1.2.1 of the National Center for Atmospheric Research. It includes the Community Atmosphere
 191 Model (CAM4) (Neale et al., 2013), the Community Land Model (CLM4; Hunke and Lipscomb,
 192 2010), the Parallel Ocean Program (POP2; Smith et al., 2010), the Community Ice Sheet Model
 193 and the Community Ice code (Glimmer-CICE4). Both the Ice sheet Model and the dynamic
 194 vegetation module (Lawrence et al., 2011) incorporated in CLM4 are switched off in this study.
 195 The horizontal resolution used is 1.9°(latitude) × 2.5° (longitude) for CAM4 with 26 vertical
 196 levels and CLM4 has identical horizontal resolution. CESM has been extensively used for
 197 modern and the tectonic climate studies (Chen et al., 2014; Goldner et al., 2014; Frigola et al.,
 198 2018). In general, this model simulates modern surface temperature distributions and equator-
 199 to-pole temperature gradients well (Gent et al., 2011), although biases exist (Neale et al., 2013).
 200 However, it strongly overestimates the Miocene meridional temperature gradient compared to
 201 reconstructions, a thorny problem for Miocene modeling practice (Burls et al., 2021;
 202 Steinthorsdottir et al., 2021) mainly caused by the inability of climate models to reproduce polar
 203 amplified warmth (Krapp and Jungclaus, 2011; Herold et al., 2011; Goldner et al., 2014; Burls
 204 et al., 2021). Nevertheless, the temperature biases in low latitudes are small, generally within
 205 1°C (Burls et al., 2021).

a mis en forme : Couleur de police : Automatique
 a mis en forme : Couleur de police : Automatique

a supprimé: CLM4 incorporates a
 a supprimé: which is

a mis en forme : Couleur de police : Automatique
 a mis en forme : Couleur de police : Automatique
 a mis en forme : Couleur de police : Automatique

a mis en forme : Couleur de police : Automatique
 a mis en forme : Couleur de police : Automatique
 a mis en forme : Couleur de police : Automatique

a supprimé:
 a mis en forme : Couleur de police : Automatique

213 **2.2. Boundary conditions**

214 Our Miocene experiments are configured with geography, topography, bathymetry and
215 vegetation cover from Frigola et al. (2018, henceforth F18), which provides boundary
216 conditions for modeling studies with a focus on the Middle Miocene. According to F18, the
217 most prominent geographic differences between the Middle Miocene and present day are the
218 opening of the Tethys, Indonesian and Panama seaways, the closure of the Bering Strait and
219 lower elevations of most of the highest regions of the globe. For instance, the African
220 topographies were reduced to 25% of its current elevation (Figs. 1a and b).

221 The topography of the Tibetan Plateau in F18 is set to its estimated Early to Middle
222 Miocene elevation. The southern and central plateau reached a near modern elevation, the
223 northern plateau is set to 3-4 km but its northward extend is reduced to reflect the rapid uplift
224 occurring in Pliocene (Harris, 2006, and the references therein). The HM reached to 60-80% of
225 its present height. As for the IP, here we lumped together all the mountain ranges west of the
226 Himalayan, including the Hindu Kush region and Pamir as the IP. In F18, the northern part of
227 the IP reached a near modern elevation as 1000-2000 m, but its southern part was lower than
228 1000 m.

229 The Miocene vegetation is prescribed as that in F18, which is a global gridded distribution
230 (Figure S1 in Supplementary Materials (SM)) merging previous reconstructions (See F18 for
231 more details). During the Miocene, vegetation types associated with lower latitudes today
232 encroached on higher latitudes. There was reduced presence of ice compared to modern
233 conditions, and ice-free regions were covered by tundra in Antarctica while cold mixed forests
234 spread over Greenland.

235 **2.3. Experimental design**

236 We first perform two simulations: the pre-industrial (piControl) and the Middle Miocene
237 (MMIO) simulation, which differ in their applied geography (Figs. 1a and b), bathymetry,
238 vegetation cover and the CO₂ concentrations while the solar constant, orbital configuration and
239 the concentrations of other greenhouse gases are kept at their modern values. The CO₂
240 concentration is set to 280 ppmv in the piControl (Eyring et al., 2016) and 400 ppmv in the
241 MMIO following the setting of F18. The choice of 400 ppmv is somewhat low but within the
242 range of published estimates (see details in F18 and Burls et al., 2021). Both simulations are
243 integrated to reach quasi-equilibrium, particularly the MMIO experiment is integrated ca. 3000

a supprimé: The

a supprimé:

a mis en forme : Couleur de police : Automatique

a mis en forme : Couleur de police : Automatique

a supprimé: over

a mis en forme : Couleur de police : Automatique

247 years. The difference between MMIO and piControl provides the background information of
248 the simulated changes in the SASM between the two periods.

a mis en forme : Couleur de police : Automatique

249 Starting from the MMIO simulation, we run a set of experiments with altered orography
250 in the HM and the IP. We examine the joint effects of the HM and IP on the SASM assuming
251 the HM and the IP rise simultaneously from flat (0%) to 100% of their reference height (Figs.
252 1c and d). The reference height is the modern altitude for the HM and the reconstructed Miocene
253 altitude for the IP. The experiments are referred as IP0HM0 and IP100HM100, respectively.
254 To further separate the climatic effect of the IP and HM uplift, we conduct another two
255 experiments: IP100HM0 and IP0HM100. In the former (latter) experiment, the HM (IP) is
256 absent while the IP (HM) reaches its reference height (Figs. 1e and f). Combined with the
257 experiments of IP0HM0 and IP100HM100, the effect of elevated IP and HM is estimated (see
258 section 3.2). To further reveal the impact of the IP uplift on the SASM evolution, two other
259 experiments are conducted: IP50HM0 and IP50HM100, indicating that the IP is reduced by
260 half of its Miocene height while the HM is absent and fully uplifted, respectively.

a supprimé: Based on

a mis en forme : Couleur de police : Automatique

261 To clarify the relative role of CO₂ forcing on SASM rainfall in the Middle Miocene, we
262 also run a set of CO₂ sensitivity experiments with the CO₂ setting to 280, 560, 800 and 1000
263 ppmv, referred to as MMIO280, MMIO560, MMIO800 and MMIO1000, respectively. The
264 high values as 800 and 1000 ppm are chosen because new reconstructions of CO₂ are generally
265 corresponded to 3 times the pre-industrial levels (Rae et al., 2021). These experiments share
266 the same boundary conditions as the MMIO simulation, differing only in CO₂ concentration.

a supprimé: pCO₂

a supprimé: pCO₂

a supprimé: pCO₂

a supprimé: correspond

267 The simulations considered in our study are listed in Table 1. The sensitivity experiments
268 are integrated from the MMIO equilibrium state for another 200 (500) years for the topography
269 (CO₂) sensitivity experiments to reach quasi-equilibrium. The final 50 years of these
270 simulations are used for analysis.

271 2.4. South Asian Summer Monsoon indices

a mis en forme : Couleur de police : Automatique

272 The following indices are defined to illustrate features of the SASM changes. ▲

a mis en forme : Couleur de police : Automatique

273 (1) All Indian rainfall (AIR): regional summer mean precipitation over the land points
274 within the domain of 7-30°N, 65-95°E. It represents the precipitation in the core region of the
275 SASM.

276 (2) Webster-Yang Index (WYI; Webster and Yang, 1992): meridional wind stress shear
277 between 850 hPa and 200 hPa averaged over 40-110°E, 0-20°N during June-August.

a supprimé: et al.,

284 (3) Somali jet strength (SMJ; Sarr et al., 2022): Maximum intensity of the Somali jet over
285 the Arabian Sea (averaged over 30-60°E, 0-20°N) during June-August.

286 2.5. Moisture budget analysis

287 Moisture budget analysis (MDA) can decompose the precipitation change into changes in
288 evaporation and moisture advection (Chou et al. 2009). It relates the net precipitation
289 (precipitation minus evaporation; P - E) to the vertically integrated moisture flux convergence
290 (Chou et al., 2009). More details about MDA are given in SM 2. This method has been widely
291 applied to paleoclimate studies in recent years, such as distinguishing the physical processes
292 involved in precipitation changes in Mid-Holocene (Sun et al., 2023). Here, we apply MDA to
293 reveal the physical processes related to SASM precipitation responses to the uplift of IP-HM
294 and to CO₂ change.

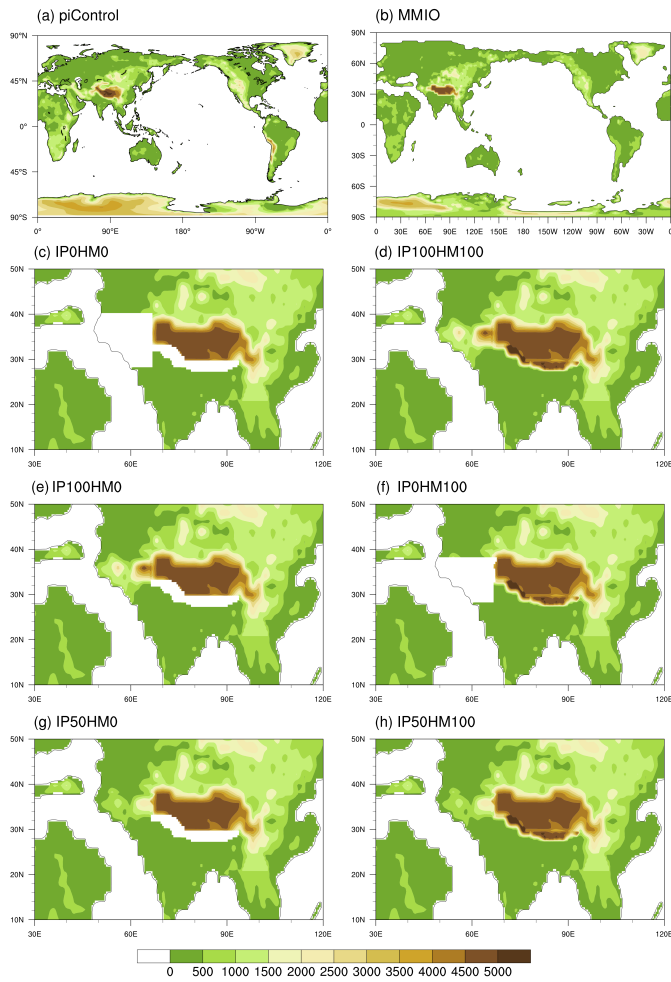
a mis en forme : Couleur de police : Automatique

a mis en forme : Couleur de police : Automatique

a mis en forme : Couleur de police : Automatique

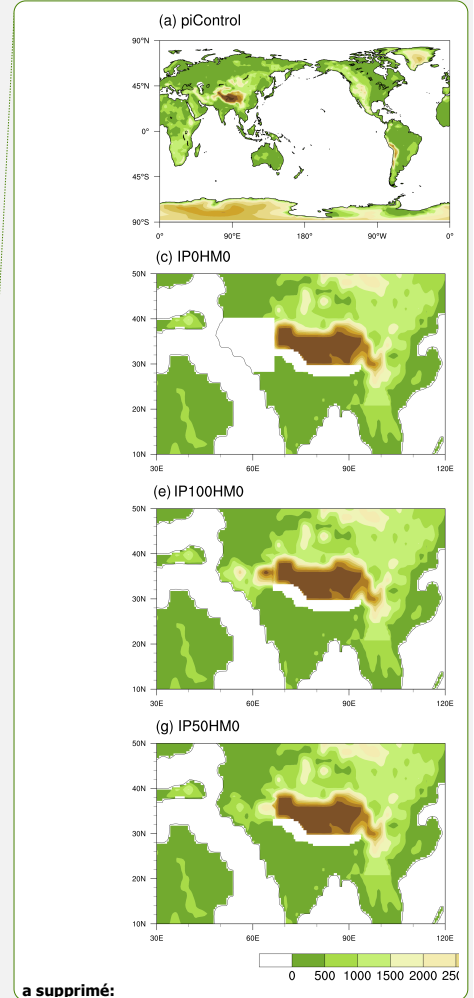
a supprimé: pCO₂

a mis en forme : Couleur de police : Automatique



296

297 **Figure 1.** Topography of (a) piControl, (b) MMIO and orographic sensitivity experiments,
 298 including (c) IP0HM0, (d) IP100HM100, (e) IP100HM0 and (f) IP0HM100, (g) IP50HM0, (h)
 299 IP50HM100 (The maps are plotted at $0.5^\circ \times 0.5^\circ$ resolution. The same maps but at $1.9^\circ \times 2.5^\circ$
 300 resolution are provided in the SM as Fig. S2).



a supprimé:

a mis en forme : Couleur de police : Automatique

a supprimé: °x0

a supprimé: °x2

a supprimé:

a mis en forme : Couleur de police : Automatique

305 **3. Results**

306 **3.1. Climatology of the SASM in the present day and Middle Miocene**

307 The CESM1.2 is one of the best models in simulating the present-day SASM (Anand et
308 al., 2018; Jin et al., 2020). The CESM1.2 reproduced the broad features of the SASM system
309 including the onshore flows and strong monsoonal precipitation when compared to the
310 observational datasets including GPCP (precipitation) and ERA5 (circulation) (Huffman et al.,
311 2009; Hersbach et al. 2020). The maximum centers of precipitation are reasonably captured
312 over the southern slope of the HM, the East Arabian Sea and Bay of Bengal despite biases in
313 intensity and extensions (Figs. 2a, b), which is largely due to the coarse spatial resolution
314 (Acosta and Huber, 2017; Anand et al., 2018; Botsyun et al., 2022a, b; Boos and Hurley, 2012).
315 Thus, we focus on the large-scale circulations and treat the local features with caution. The
316 regional summer mean precipitation, as measured by the AIR, is 7.7 mm day⁻¹ in GPCP and
317 8.7 mm day⁻¹ in the piControl experiment. The positive bias reflects an overestimation of
318 precipitation in the Western Ghats and at the HM foothills.

319 Compared with the piControl experiment, the MMIO simulation displays apparent
320 adjustment of the JJA mean low-level circulation. The westerlies pass Africa into the Indian
321 region, and a cyclonic circulation develops over the Arabian Sea, the cross-equatorial flow
322 weakens and displaces southward (Fig. 2c). There is considerable enhancement of monsoonal
323 precipitation in South Asia but not limited there (Fig. 2c). AIR in MMIO simulation is 10.4 mm
324 day⁻¹, which is ~20% higher than that in piControl experiment.

325 The wetter Miocene climate is also reflected by the widespread Africa-Asian monsoon,
326 which was suggested by previous modeling studies (Herold and Huber, 2011; Zhang et al.,
327 2015). Here a monsoon-like climate is defined as local summer-minus-winter precipitation
328 exceeding 2 mm day⁻¹ and the local summer precipitation exceeding 55% of the annual total
329 (Wang and Ding, 2008). This monsoon index is determined by the intensity of summer
330 monsoonal precipitation in the region of the South Asian Monsoon (SAM). Compared with
331 present day, the domain of the SAM extends westward both in land and over the Arabian Sea
332 where it nearly connects the African monsoon (Fig. 3c). Interestingly, this characteristic is also
333 noted in the Miocene study of Fluteau et al. (1999), despite significant differences in the climate
334 model and paleogeography employed in the two studies. The distribution of the simulated SAM
335 is generally consistent with the proxies (Table 2), confirming the wide existence of SAM in the
336 Middle Miocene in terms of rainfall seasonality.

a mis en forme : Couleur de police : Automatique

a mis en forme : Couleur de police : Automatique

a mis en forme : Couleur de police : Automatique

a supprimé:), a feature

a mis en forme : Couleur de police : Automatique

a supprimé: presented

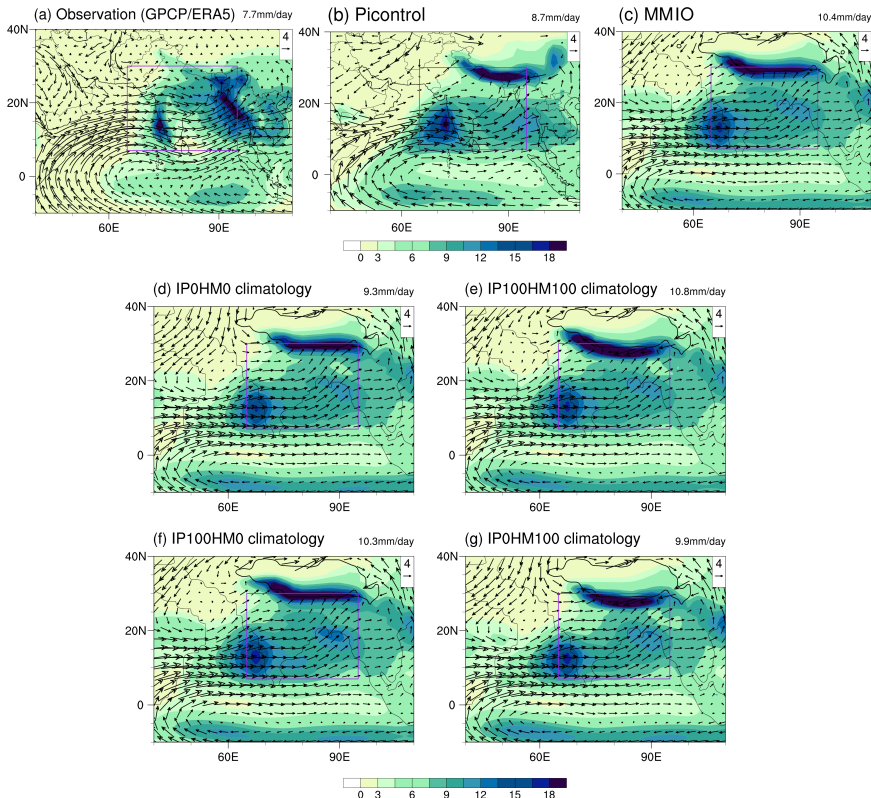
a mis en forme : Couleur de police : Automatique

a supprimé:)

a mis en forme : Couleur de police : Automatique

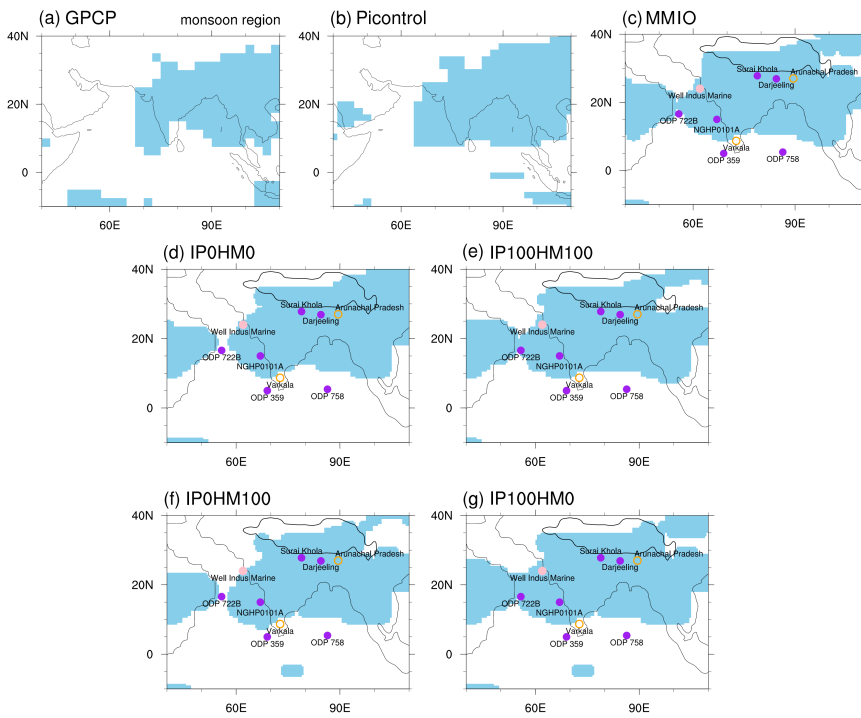
a supprimé:

a mis en forme : Couleur de police : Automatique



341
 342 **Figure 2.** Climatology of JJA (June-July-August) seasonal mean South Asia summer monsoon
 343 (SASM) precipitation (mm day^{-1}) and 850 hPa winds (vectors, m s^{-1}) from (a) observation
 344 precipitation from GPCP and circulation from ERA5), (b) Preindustrial control experiment and
 345 (c) MMIO experiment. (d) IP0HM0, (e) IP100HM100, (f) IP100HM0, (g) IP0HM100.
 346 Climatology is the average over 1979-2005 for the observation. As for the piControl and MMIO
 347 experiment, we select the last 50 and 100 years of simulation, respectively. All Indian rainfall
 348 (AIR) is shown at the top-right of each panel. AIR indicates precipitation over the land points
 349 within the purple square in each panel (7-30°N, 65-95°E). The black contour in panel (c)-(g)
 350 indicates the altitude of 2500 m.

a mis en forme : Couleur de police : Automatique



351
 352 **Figure 3.** The monsoon domains (blue shading) in (a) GPCP, (b) piControl experiment, (c)
 353 MMIO experiment, (d) IP0HM0, (e) IP100HM100, (f) IP0HM100 and (g) IP100HM0
 354 experiments, which are defined by the regions where local summer-minus-winter precipitation
 355 exceeds 2 mm day^{-1} and the local summer precipitation exceeds 55% of the annual total. Dots
 356 in (c-g) represent reconstructions near the SASM region, purple solid dots denote enhanced
 357 SASM, orange circles denote no significant change and pink solid dots denote weakened SASM
 358 from middle to late Miocene. The black contour in panel (c)-(g) indicates the altitude of 2500
 359 m.

360 3.2. The effect of the HM and IP uplift

361 We first examine the effect of the joint uplift of the HM and IP (hereafter referred to as
 362 IP-HM). With the uplift of the IP-HM (Fig. 4a), a prominent cyclonic anomaly is built to the
 363 west of the IP with the intensified southwesterlies from Africa via the Arabian Sea into the
 364 northwestern India. Increased precipitation is found along the eastern flank of the cyclonic
 365 anomaly to the slopes of the western HM and northeastern IP. In the eastern part of the monsoon

a supprimé: ¶

a mis en forme : Couleur de police : Automatique

a mis en forme : Couleur de police : Automatique

a mis en forme : Couleur de police : Automatique

a supprimé: ¶

a mis en forme : Couleur de police : Automatique

a supprimé: This anomaly regarded as the deepening of thermal low is also shown in previous study (Sarr et al., 2022).

370 region, the enhanced precipitation occurs mainly along the southern edge of the HM while the
371 leeward side features a remarkably decreased precipitation, indicating the rain shadow effect.

372 Corresponding to the summer precipitation change in response to IP-HM uplift, the
373 domain of the SASM expands westward over the Arabian Sea and the Indian subcontinent (Figs.
374 3d-e). The western extension over land is about 65°E in the IP0HM0 experiment and reaches
375 60°E in the IP100HM100 experiment, indicating that the change of the SASM is significant in
376 the northwest of the Indian subcontinent. Interestingly, monsoonal signal exists in the IP0HM0
377 experiment, an analogue to the “early Miocene”, indicating that proto-monsoon exists by
378 having TP only, which is also found in previous studies (Sarr et al., 2022). At the site of ODP
379 722B, monsoonal signal is absent in IP0HM0 (Fig.3d), but present in IP100HM80 (MMIO, Fig.
380 3c) and IP100HM0 (Fig. 3e) when the IP-HM is uplifted.

381 We further separate the effect of the IP and HM uplift. The climate response to IP uplift
382 (IP100-IP0) is estimated as $((IP100HM0-IP0HM0)+(IP100HM100-IP0HM100))/2$. Similarly,
383 the effect of HM uplift HM100-HM0 is estimated as $((IP0HM100-IP0HM0)+(IP100HM100-$
384 $IP100HM0))/2$. The changes in precipitation and low-level circulation much resemble that
385 attributing to the IP-HM uplift (Fig. 4a), indicating that by itself, the IP can sustain major parts
386 of the precipitation changes except over the central-eastern HM. The easterly anomaly across
387 the Indian subcontinent indicates that the westerly is blocked by elevated IP from north India,
388 facilitating moisture convergence and rainfall increase over the northern Indian continent. As a
389 result, the regional mean precipitation increases by 1.1 and 2.0 mm/day over the core (7-30°N,
390 65-95°E) and western regions (15-35°N, 50-75°E), respectively.

391 In contrast to the widespread effect of the IP on the SASM, the HM uplift only has a local
392 effect (Fig. 4c), which is mostly confined to the HM and its close vicinity, and the change in
393 low level circulation is noisy and weak. The precipitation strongly increases along the southern
394 slope of the HM and dramatically decreases on its leeward side, resembling the changes in
395 precipitation in the eastern region caused by the IP-HM uplift. As a result, there is little change
396 in the regional mean precipitation over the core and eastern regions (15-35°N, 75-95°E).
397 Specially, the changes in precipitation patterns and low-level circulation between IP100HM100
398 and MMIO (not shown) closely resemble that shown in Fig. 4c, albeit with reduced intensity,
399 indicating that further uplift of HM above the TP does not result in intensified SASM.

a mis en forme : Couleur de police : Automatique

a supprimé: IPHM0

a mis en forme : Couleur de police : Automatique

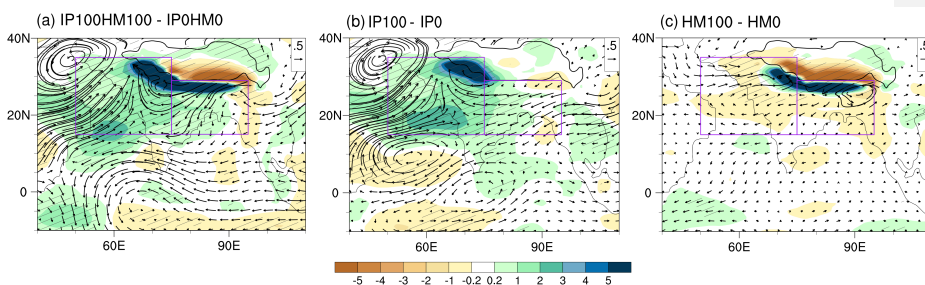
a mis en forme : Couleur de police : Automatique

a mis en forme : Couleur de police : Automatique

a mis en forme : Couleur de police : Automatique

401 In summary, the joint influences of the IP-HM uplift on the SASM are the superimposed
 402 effect of the IP and HM. In the western region, i.e., from the Arabian Sea to the northwestern
 403 India and Pakistan, the IP plays a dominant role while in the eastern region, i.e., the east part of
 404 South Asia, the changes in the SASM mainly attribute to the HM uplift. And the western
 405 extension of the SASM domain over the Arabian Sea and the Indian subcontinent is mainly
 406 caused by the uplift of IP rather than HM (Figs. 3f-g).

a mis en forme : Couleur de police : Automatique



407

408 **Figure 4.** Precipitation (shaded, mm day⁻¹) and 850hPa wind differences between (a)
 409 IP100HM100 and IP0HM0 experiments; (b) IP100 and IP0 experiments; (c) HM100 and HM0
 410 experiments. Here $IP100-IP0 = ((IP100HM0-IP0HM0) + (IP100HM100-IP0HM100))/2$,
 411 $HM100-HM0 = ((IP0HM100-IP0HM0) + (IP100HM100-IP100HM0))/2$. The black contour in
 412 each panel indicates the altitude of 2500 m. Purple boxes represent west (15-35°N, 50-75°E)
 413 and east (15-29°N, 75-95°E) parts of the South Asian monsoon region. Slashes indicate
 414 values >95% confidence level based on the *Student's t* test.

415 3.3. The effects of the CO₂ forcing vs topographic forcing

416 To illustrate the effect of CO₂ forcing on SASM during the MMIO, we show the
 417 climatology of the SASM at low and high levels of CO₂ concentration based on MMIO28 and
 418 MMIO1000 experiments, respectively (Fig.5). The spatial circulation patterns in these two
 419 experiments are similar to that in the MMIO but the magnitudes change significantly (Fig.5a
 420 and b, Fig.2c). With the increase of CO₂, the meridional cross-equatorial flow slightly
 421 strengthens along the East Africa coast until 15°N but weakens to its east (Fig. 5c, d), leading
 422 to little change in the regional mean strength of this flow over the Arabian Sea. Meanwhile,
 423 precipitation enhances along the band of 15-25°N but decreases to its south, indicating a
 424 northward shift of the tropical rainfall belt. As the CO₂ rises from 280 ppm to 400 ppm, and
 425 subsequently to 1000 ppm, the AIR index correspondingly increases by 0.5 mm day⁻¹ and 1.2

a supprimé: pCO2

a supprimé: pCO2

a supprimé: pCO2

a supprimé: west

a supprimé: pCO2

431 mm day⁻¹, respectively. MBA (SM2) further reveals that the increased monsoonal precipitation
432 is primarily induced by enhanced thermodynamic conditions due to atmospheric warming,
433 while the contribution from the change in large-scale monsoon circulation plays a secondary
434 role (SM Fig S5c and d). For instance, the precipitation change between MMIO1000 and
435 MMIO in the core SASM region is 1.2mm/day, of which 0.6 is from the thermodynamical
436 processes related to changes in moisture and 0.25 mm/day from the dynamical processes related
437 to circulation change.

a supprimé: Similar conclusion is also reported in projecting future climate change facing the rising CO₂ (Endo and Kitoh, 2014).

a mis en forme : Barré

a supprimé: pCO₂

438 To compare the effect of CO₂ forcing versus topographic forcing on the SASM, we
439 examine the changes of precipitation and low-level circulations between MMIO1000 and
440 IP0HM0 experiments (Fig. 5e), which actually reflects the combined effects of the CO₂ forcing
441 (MMIO1000-MMIO) and IP-HM uplift (MMIO-IP0HM0). It is clear that the SASM changes
442 in Fig. 5e bear the features of Fig. 5d and Fig. 4a: precipitation enhancing along the band of 15-
443 25°N and reducing to its south in response to increased CO₂ and a prominent cyclonic anomaly
444 built to the west of the IP in response to the IP-HM uplift. Moisture budget analysis further
445 reveals that the enhanced precipitation of 3.2 mm day⁻¹ in the west part of the SAM region is
446 equally attributed to the vertical and horizontal moisture advection of 2.3 mm day⁻¹ (Fig. 6).
447 The moisture advection by anomalous meridional winds is the dominant contribution term,
448 which is actually the response to the IP uplift as we see in next section.

a supprimé: pCO₂

449 We further examine the impacts of CO₂ forcing and topographic forcing in terms of WYI,
450 SMJ, AIR (Sect. 2.4) and the mean precipitation over the western part of the SASM region
451 (Fig.7). Under the topographic forcing, WYI exhibits small changes, with the exception of a
452 relatively lower value in the IP0HM100 experiment. Concurrently, both precipitation and low-
453 level circulation indices increase in response to the IP uplift, indicating a quasi-circulation-
454 rainfall coupling relationship. With the increasing of CO₂ forcing, there is a noticeable decrease
455 in WYI, whereas AIR and precipitation in the western SAM region increase significantly,
456 indicating a decoupling relationship between large-scale circulation and monsoonal rainfall.
457 The cross-equator flow at lower level (Somali Jet) is insensitive to CO₂ change as already
458 shown in Fig.5.

a supprimé: pCO₂

a supprimé: pCO₂

a supprimé: pCO₂

459 The maximum difference of each index across the set of CO₂ or topographic sensitivity
460 experiments is defined as the effect of each driver. In terms of WYI (Fig. 7a), the effect of CO₂
461 forcing is ~150% greater than that of IP-HM forcing, with values of 2.5 m s⁻¹ vs 1.0 m s⁻¹.
462 According to the AIR, the influence of CO₂ forcing is ~1.5 mm day⁻¹, which is comparable to

a mis en forme : Couleur de police : Automatique

a supprimé: pCO₂

a supprimé: pCO₂

a supprimé: pCO₂

473 that of IP-HM forcing ($\sim 1.5 \text{ mm day}^{-1}$) but is larger than the individual contributions of IP
474 forcing ($\sim 1.0 \text{ mm day}^{-1}$) and HM forcing ($\sim 0.5 \text{ mm day}^{-1}$). In the western region, the effect of
475 CO_2 forcing is about 75% compared to that of IP forcing (~ 1.5 vs $\sim 2.0 \text{ mm day}^{-1}$). In summary,
476 CO_2 forcing is the dominant driver for large-scale monsoon circulation, while the uplift of the
477 IP exerts a more significant effect on regional circulation and the associated precipitation.

478 We note that the SASM response to CO_2 forcing in the Middle Miocene is very similar to
479 that of projecting future climate change. For instance, increased SASM precipitation occurring
480 with decreased WYI is also projected under abrupt quadrupling of CO_2 (Kong et al., 2022). The
481 low-level monsoon circulations are projected to slightly weaken, consistent with the little
482 change in the intensity of low-level cross-equator flow in our Miocene simulations (Fig.5 and
483 6). Based on an analysis across 20 climate models, Endo and Kitoh (2014) concluded that in a
484 warmer world, projected increase in SASM precipitation is mainly attributed to thermodynamic
485 processes. This finding aligns with our MBA result (Fig.5). The similarity in the SASM
486 response to changes in CO_2 implies the presence of a comparable physical mechanism operating
487 during the two warm periods.

a supprimé: ,

a supprimé: pCO2

a supprimé: pCO2

a mis en forme : Couleur de police : Automatique

a mis en forme : Couleur de police : Automatique

a mis en forme : Couleur de police : Automatique, Indice

a mis en forme : Couleur de police : Automatique

a mis en forme : Couleur de police : Automatique

a mis en forme : Couleur de police : Automatique

a mis en forme : Couleur de police : Automatique

a supprimé: of

a mis en forme : Couleur de police : Automatique

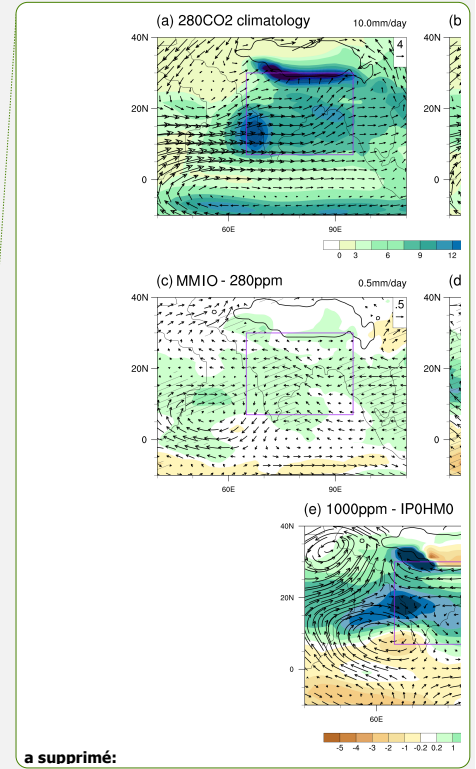
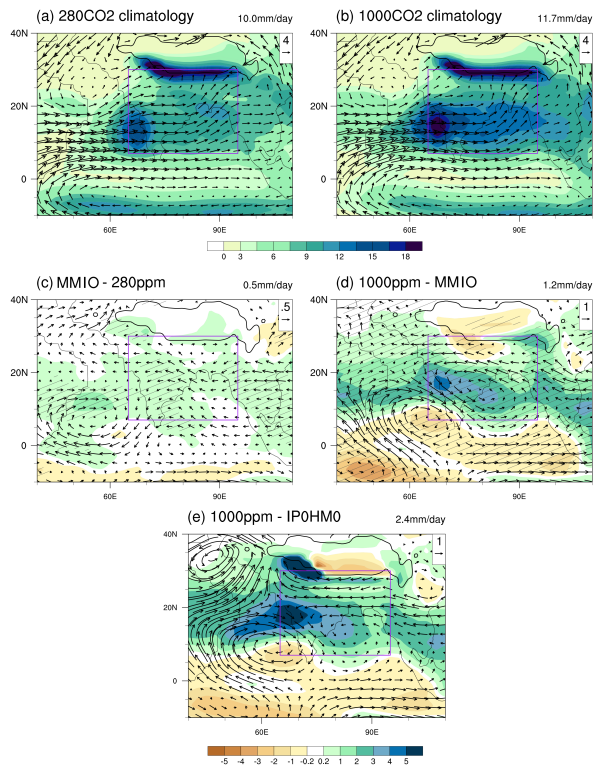
a mis en forme : Couleur de police : Automatique

a supprimé: change suggests a similar

a mis en forme : Couleur de police : Automatique

a supprimé: in

a mis en forme : Couleur de police : Automatique



a supprimé:

494

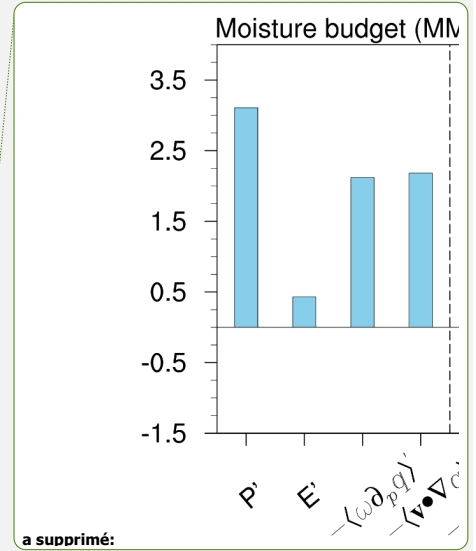
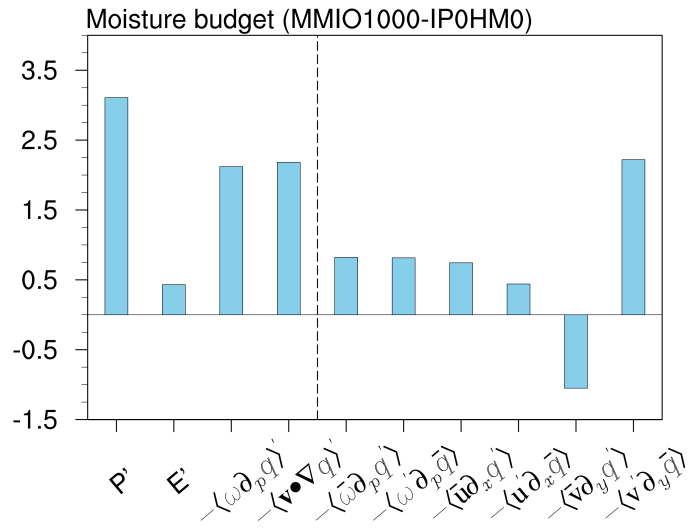
495 **Figure 5.** Climatology of JJA (June-July-August) mean South Asia summer monsoon (SASM)
 496 precipitation (mm day^{-1}) and 850 hPa winds (vectors, m s^{-1}) from (a) MMIO_280 experiments,
 497 and (b) MMIO_1000 experiments. Precipitation (shaded, mm day^{-1}) and 850hPa wind
 498 differences (vector, m s^{-1}) between (c) MMCO and MMCO_280 experiments; (d)
 499 MMCO_1000 and MMCO experiments; (e) MMIO_1000 and IP0HM0 experiments.

a mis en forme : Couleur de police : Automatique

a mis en forme : Couleur de police : Automatique

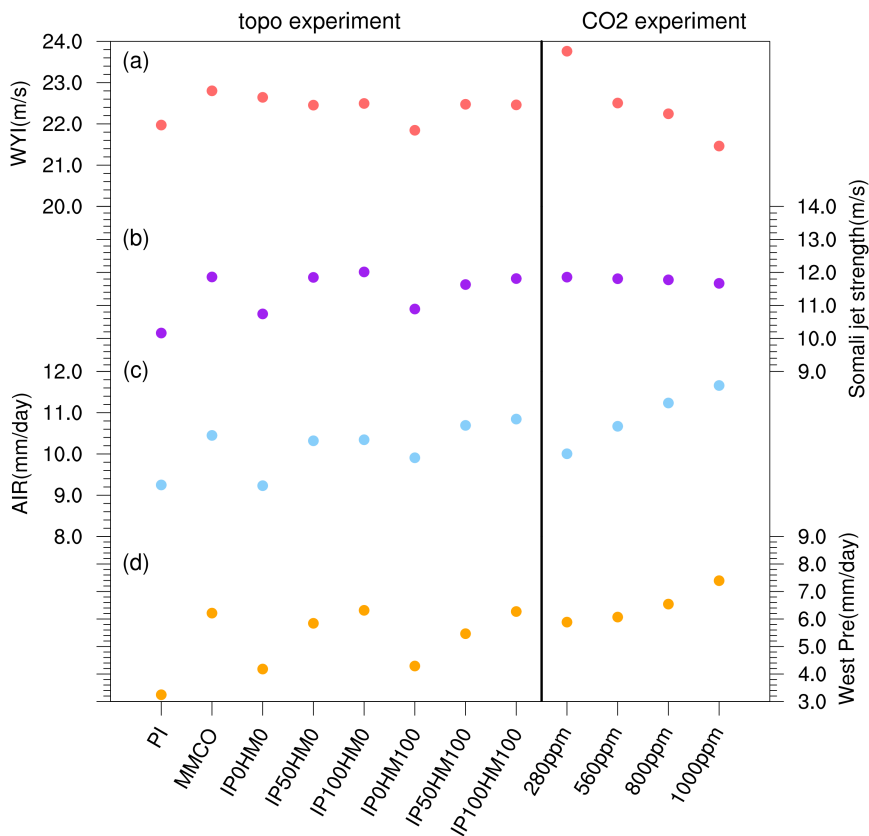
a mis en forme : Couleur de police : Automatique

a mis en forme : Couleur de police : Automatique



501

502 **Figure 6.** Moisture budget for regional mean precipitation differences (mm day⁻¹) over the
 503 west part (15-35°N, 50-75°E) of the South Asian monsoon region between MMIO1000ppm
 504 and IP0HM0 experiments.



506

507 **Figure 7.** South Asian summer monsoon circulation and precipitation response in sensitivity
 508 experiments. Left, topography experiments. Right, CO₂ experiments. (a) Webster-Yang Index
 509 (meridional wind stress shear between 850 hPa and 200 hPa averaged over 40-110°E, 0-20°N
 510 during June-August). (b) Maximum intensity of the Somali jet over the Arabian Sea (averaged
 511 over 30-60°E, 0-20°N during June-August). (c) Regional mean precipitation over the land
 512 points within the domain (7-30°N, 65-95°E), named All indian rainfall (AIR). (d) Precipitation
 513 over the western part of South Asian summer monsoon region.

514 **4. Mechanisms of the IP uplift on the SASM precipitation**

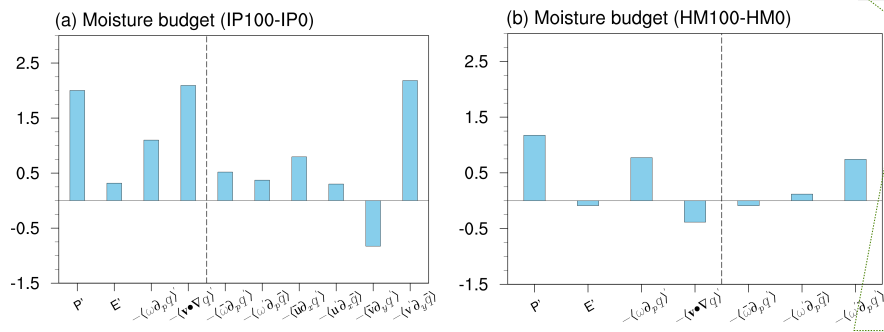
515 To understand the mechanism of increased precipitation caused by IP uplift and HM uplift,
 516 we first use the moisture budget decomposition to identify the major moisture contributors.

517 Here we provide the main analysis results (Fig.8), more details are seen in SM2. To focus our

a mis en forme : Couleur de police : Automatique

a mis en forme : Couleur de police : Automatique

518 analyses on atmospheric dynamics, we neglect the contribution of evaporation, which is
 519 relatively small in our simulation despite the possibly important role for precipitation in the
 520 northwest India (Zhang et al., 2019). In response to IP uplift, the increased precipitation (2.0
 521 mm day⁻¹) is largely attributed to the horizontal moisture advection (2.1 mm day⁻¹), in particular
 522 the moisture advection by anomalous meridional winds, while the vertical advection plays a
 523 secondary role (1.1 mm day⁻¹). In response to HM uplift, precipitation change (ca 1.2 mm day⁻¹)
 524 is mainly caused by the vertical moisture advection (0.9 mm day⁻¹) and is offset by the
 525 horizontal moisture advection (-0.4 mm day⁻¹). Its dominant contributor is a nonlinear term
 526 involving strong interaction between the vertical motion anomalies and moisture change (See
 527 SM2).



528 **Figure 8.** Moisture budget for regional mean precipitation differences (mm day⁻¹) over (a) the
 529 west part (15-35°N, 50-75°E) of the South Asian monsoon region between IP100 and IP0
 530 experiments, (b) the east part (15-29°N, 75-95°E) of the South Asian monsoon region between
 531 HM100 and HM0 experiments.
 532

533 We then examine the responses of the monsoon relevant variables to the uplifts of the IP
 534 and HM and the involved physical processes with focus on the effect of the IP. With IP uplift,
 535 the airs of high equivalent potential temperature (θ_e) at lower troposphere are accumulated in
 536 the IP and the surrounding region (Fig. 9a). The increased θ_e attributes to the enhancement of
 537 specific humidity (Fig. 9b) as moisture is advected by the anomalous southwesterly from North
 538 Africa via the Arabian Sea into the northwestern India and Pakistan (Fig. 9b), meanwhile it
 539 increases the convective instability. Triggered by surface sensible heating (Wu et al., 2012;
 540 Medina et al., 2010), convection takes place. At 500hPa, the upward motion anomalies are
 541 found over the IP and along the HM (Fig. 9c), reflecting the lifting effect of the elevated
 542 topography. The height of the lifted condensation level (LCL) is significantly reduced over the
 543

a mis en forme : Couleur de police : Automatique

a mis en forme : Couleur de police : Automatique

a mis en forme : Couleur de police : Automatique

a mis en forme : Couleur de police : Automatique

a mis en forme : Couleur de police : Automatique

a mis en forme : Couleur de police : Automatique

a mis en forme : Couleur de police : Automatique

a supprimé:

a mis en forme : Couleur de police : Automatique

a mis en forme : Couleur de police : Automatique

a mis en forme : Couleur de police : Automatique

a mis en forme : Couleur de police : Automatique

a mis en forme : Couleur de police : Automatique

a mis en forme : Police : Times New Roman, 12 pt

a mis en forme : Couleur de police : Automatique

a supprimé: southeasterly

a mis en forme : Couleur de police : Automatique

a supprimé: north

a mis en forme : Couleur de police : Automatique

a mis en forme : Couleur de police : Automatique, Non Barré

a mis en forme : Couleur de police : Automatique

547 IP and along the western edge of the HM (Fig. 9d), which is likely resulted from the elevated
 548 surface sensible heating (He, 2017). Reduced LCL facilitates the moist convection to occur,
 549 further warming the air parcels by the released latent heating. Consequently, specific humidity
 550 and θ_e further increase in the middle troposphere (Fig. 9e), which in return favors the convection
 551 activity. The pattern match between the specific humidity and θ_e indicates that the increased θ_e
 552 is primarily contributed by the increase of specific humidity then by the warming (Fig.9c). At
 553 the upper troposphere, forced by the latent heating, the warm-centered South Asian High
 554 strengthens over the IP (Fig. 9f), which is coupled with the cyclonic anomaly at low level (Fig.
 555 9b), leading to moisture convergence over the western region and accelerate the convection
 556 activity. Positive feedback is thus built between precipitation and circulation. Regarding HM
 557 uplift, there is not a circulation adjustment between the low and high levels, the precipitation-
 558 circulation coupling thus cannot be built.

559 In this thermodynamical process, the IP's blocking/mechanical effect is also noticeable as
 560 it blocks the cold dry extratropical airs from northern India where the airs of high θ_e cumulate
 561 (Fig. 9a). However, this effect is relatively weak given the small contribution of the easterly
 562 anomaly to precipitation increase (less than 0.3 mm day^{-1} , see Fig. 8a: $-\langle u' \partial_x \bar{q}_t \rangle$) according
 563 to the moisture budget.

a mis en forme : Couleur de police : Automatique

a mis en forme : Couleur de police : Automatique

a mis en forme : Couleur de police : Automatique

a supprimé: to

a mis en forme : Couleur de police : Automatique

a mis en forme : Couleur de police : Automatique

a mis en forme : Couleur de police : Automatique

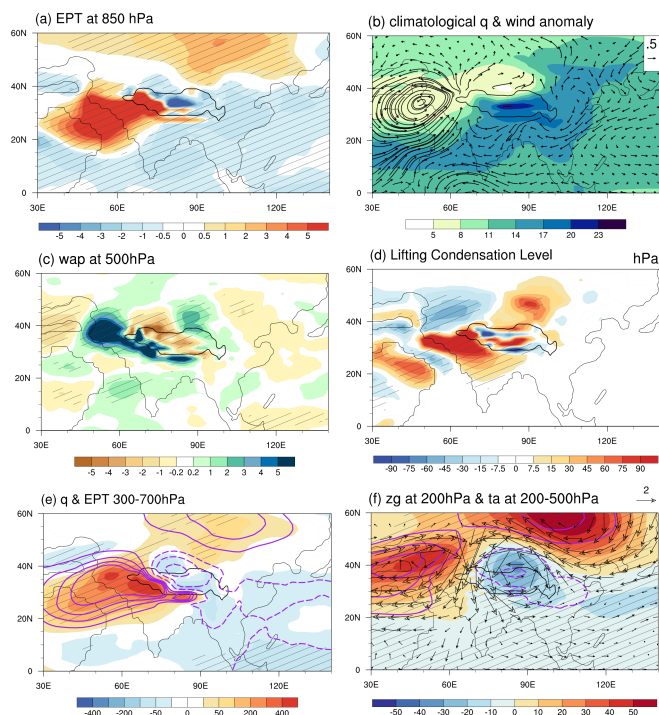
a mis en forme : Couleur de police : Automatique

a mis en forme : Couleur de police : Automatique

a mis en forme : Couleur de police : Automatique

a mis en forme : Couleur de police : Automatique

a mis en forme : Couleur de police : Automatique



565
 566 **Figure 9.** The differences of JJA mean thermal dynamical and dynamical variables between
 567 IP100HM100 and IP0HM0 simulations. (a) Equivalent Potential temperature (EPT, shading,
 568 unit: K) at 850 hPa; (b) climatological specific humidity q (shading, g/kg) and wind differences
 569 (vector, unit: m s^{-1}) at 850 hPa; (c) vertical velocity w_{ap} in pressure coordinate (-10^{-2} Pa/s) at
 570 500 hPa; (d) Lifting condensation level (LCL, unit: hPa, positive value represents lower LCL);
 571 (e) Specific humidity (shading) and EPT (contours, unit: K) integrated between 300 and 700
 572 hPa; (f) geopotential height z_g (shading, unit: m), temperature anomalies (contours, unit: K)
 573 and wind (vector, unit: m s^{-1}) at 200 hPa.

574 5. Discussion

575 5.1. Application to monsoonal reconstructions

576 A remarkable intensification of the SASM in the Middle Miocene is revealed by increasing
 577 evidence (Fig. 3c; Table 2). In the western India and the Arabian Sea, monsoon-like
 578 precipitation appeared in the early Miocene (Clift et al., 2008; Reuter et al., 2013; Ali et al.,
 579 2021) and intensified at ~ 15 -12 Ma (Clift et al., 2008; Yang et al., 2020). In the eastern India,

a supprimé: represent

a supprimé: anoamlies

a mis en forme : Couleur de police : Automatique

a mis en forme : Couleur de police : Automatique

a supprimé:

a mis en forme : Couleur de police : Automatique

583 the intensification of SASM occurred at ca 15 Ma (Khan et al., 2014) to ~13-11 Ma (Bhatia et
584 al., 2021; Vogali et al., 2017). In terms of wind system, a weaker “proto-monsoon” existed
585 between 25 and 12.9 Ma (Betzler et al., 2016) and an abrupt intensification occurred at 12.9 Ma
586 inferred from the sedimentary records in the Maldives (Betzler et al., 2016) and in the western
587 Arabian Sea (Gupta et al., 2015), indicating the inception of a modern Somali Jet. Besides,
588 monsoonal upwelling thus possibly the strengthening of wind speed in the western Arabian Sea
589 was observed since ca 14.8 Ma.

590 Our modeling results support the existence of the SASM (Clift et al., 2008) in terms of
591 precipitation seasonality in early Miocene represented by the IPOHM0 experiment when the
592 proto-TP existed while the IP and HM were low (Fig.3). With the uplift of the IP rather than
593 the HM during middle Miocene, monsoonal precipitation increased in the northwest of the
594 Indian landmass as shown in the ~IP50, ~HM50 and IP100HM100 experiments (Fig.6)
595 corroborating the hypothesis that increased sedimentary and weathering fluxes between 25 and
596 15 Ma could be partially linked with monsoon intensification related to the coeval of IP-HM
597 (Clift et al., 2008). Meanwhile, with the deepening of cyclonical anomaly over the west of the
598 IP (Fig.4b), southwesterly strengthens in the western Arabian Sea, which somewhat agrees with
599 the reconstructions that suggests the inception of modern Somali Jet (Betzler et al., 2016). But
600 the inception of modern Somali Jet is more likely attributed to the uplift of the East African
601 topography demonstrated in modeling studies (Chakraborty et al., 2006; Wei and Bondoni,
602 2016; Sarr et al., 2022; Tardif et al., 2023) and/or the emergence of land in Eastern Arabian
603 Peninsula (Sarr et al., 2022). This aligns with geological evidence indicating that the East Africa
604 began to uplift in the late Oligocene–early Miocene and rapidly uplifted in the middle–late
605 Miocene (Macgregor, 2015). We conduct a series of complementary experiments (SM3) and
606 confirm that elevated East African highlands plays an essential role in producing the modern-
607 like Somali Jet. Meanwhile, it creates an anti-cyclonic anomaly over the north Arabian Sea as
608 revealed by previous studies, leading to reduced moisture transport into Indian landmass thus
609 decreased monsoonal precipitation. Therefore, there is likely a complementary and competing
610 effect on SASM evolution between the uplift of the IP and the East African highlands.

611 The enhanced precipitation at 13 Ma is inferred from leaf fossil in the eastern HM, which
612 has been attributed to the rise of the HM (Khan et al., 2014; Bhatia et al., 2021). But this
613 hypothesis cannot be supported by our sensitivity experiment. Neither can it be interpreted by
614 the uplift of the IP based on our simulations. In contrast, some modeling studies suggested

a mis en forme : Couleur de police : Automatique

a supprimé: and a major enhancement in the period 11-10 Ma (Zhuang et al., 2017).

a mis en forme : Couleur de police : Automatique

a mis en forme : Couleur de police : Automatique

a supprimé: ; Zhuang et al., 2017).

a mis en forme : Couleur de police : Automatique

a mis en forme : Couleur de police : Automatique

a mis en forme : Couleur de police : Automatique

a mis en forme : Couleur de police : Automatique

a mis en forme : Couleur de police : Automatique

a mis en forme : Couleur de police : Automatique

a supprimé: bewteen

a mis en forme : Couleur de police : Automatique

619 enhanced precipitation in along the HM in response to mountain uplift in the American region
620 and northern TP (Chakraborty et al., 2006; Miao et al., 2022). Therefore, remote impacts on
621 precipitation change in the eastern HM should be taken into account.

622 The CO₂ forcing has little impact on the intensity of the Somali Jet, indicating its little
623 contribution to the strengthening of surface wind inferred from the reconstructions (Gupta et
624 al., 2015), but its effect on precipitation is likely to superimpose on that of the IP uplift. It is
625 speculated that during the early part of the Middle Miocene Climatic Optimum, abrupt rise of
626 the CO₂ amplifies the effect of the IP uplift, leading to the markedly intensified SASM
627 precipitation around 15 Ma as depicted in reconstructions (Clift et al., 2008; Yang et al., 2020).
628 While during the mid-late Miocene, the decreasing tendency of CO₂ offsets the effect of the IP
629 uplift, although precipitation still intensifies due to the dominant impact of the latter. Given the
630 wide range of reconstructed CO₂ in terms of intensity and timing during the Middle Miocene,
631 the effect of CO₂ forcing experiences large uncertainty. Nevertheless, the CO₂ variation itself
632 cannot interpret the strengthening of wind along the Somali or the evolution of SASM
633 precipitation intensity as inferred from the reconstructions.

634 The two sites ODP 359 and 758, situated in the Inner Sea of the Maldives and the southern
635 Bay of Bengal, respectively, indicate an abrupt strengthening of monsoonal circulations in the
636 SASM regions at 12.9 Ma and 13.9 Ma, respectively. However, our modeling efforts cannot
637 replicate these enhancements through either the uplift of the IP and HM or a reduction in CO₂
638 levels. Hence, it is likely that other factors exert a more significant influence on the
639 reorganization of the SASM system. Examples include Antarctic glaciation, as suggested in Ali
640 et al. (2021; Sarr et al., 2021), as well as the closure of the Tethys, as discussed in research by
641 Betzler et al. (2016) and Bialik et al. (2019).

642 5.2. Comparison with previous modeling studies

643 Concerning the effect of uplifted HM and IP on the SASM, our modeling results confirm
644 the intensified SASM linked with the uplift of the IP (Liu et al., 2017; Zhang et al., 2015; Acosta
645 and Huber, 2020; Tardif et al., 2020, 2023) rather than the HM (Zhang et al., 2012), particularly
646 over the western region, i.e., from the Arabian Sea to the northwestern India and Pakistan.
647 When the evolution history of the HM-TP is taken into account, the uplift of the HM against
648 the TP mainly enhances the orographic precipitation along the windward side of the HM and
649 has little impact on regional monsoonal precipitation. While the effects of IP uplift from our
650 AOCGM simulations qualitatively agree with previous studies using AGCMs (Wu et al., 2012;
651 Liu et al., 2017; Zhang et al., 2015; Acosta and Huber, 2020), additional analysis (not shown)

a supprimé: pCO₂

a supprimé: pCO₂

a supprimé: pCO₂

a supprimé: pCO₂

a mis en forme : Indice

a mis en forme : Couleur de police : Automatique

a supprimé:

a mis en forme : Couleur de police : Automatique

657 reveals notable impacts on ocean circulations. These impacts are evidenced by changes in SSTs
658 and precipitation in tropical oceans, potentially influencing SASM intensity through
659 teleconnection. However, further discussion on the added value of OAGCM extends beyond
660 the scope of our current study.

661 Regarding the mechanism of the IP uplift on the SASM, our analyses tend to support its
662 thermal forcing effect (Wu et al., 2012; Liu et al., 2017), but instead of emphasizing the sensible
663 heating effect, we highlight the latent heating as a crucial link between the convection activity
664 and regional circulations as previous study (He, 2017). This demonstrates that it is not only
665 temperature, but also the hydrological cycle modifications as depicted in Section 4 must be
666 taken into account to understand the involved physical process. We also note that the IP's
667 blocking/mechanical effect is much weaker in our study than that reported in Tang et al. (2013).
668 In their study, the elevated IP effectively blocked the westerly flow to the south of the HM,
669 facilitating the moisture advection from the Bay of Bengal into northern India, thus strongly
670 enhanced the SASM precipitation, particularly in eastern India. Similar blocking effect (or role
671 of gatekeeper) is also reported by Acosta and Huber (2020). Both studies utilized high spatial
672 resolution models and were conducted using modern geographies. The weak blocking effect in
673 our study is likely due to: (1) smaller size of the IP in the Miocene than in the present day; (2)
674 spatial lower-resolution model than that used in their studies (~1° or higher), thus some critical
675 regional circulations linked to the SASM are likely misrepresented (Boos and Hurley, 2013;
676 Acosta and Huber, 2017).

677 5.3. Uncertainty and Methodological Limitation

678 Geography, particularly the land-sea distribution, is another important driver for Asian
679 monsoon development (Ramstein et al., 1997; Farnsworth et al., 2019; Sarr et al., 2022; Tardif
680 et al., 2023). The land-sea distribution used in our Miocene simulations, like other
681 reconstructions (Herold et al., 2008; He et al., 2021, and references therein) inevitably contain
682 uncertainties. For instance, the Bohai Bay and Yellow Sea basins in East Asia are open in the
683 F18, contrary to regional stratigraphy and lithofacies records (Tan et al., 2020). The Greenland-
684 Scotland Ridge in F18 is set as ~4000 m, significantly deeper than a middle bathyal
685 environment (<1000-m deep) indicated by geological evidence (Stocker et al., 2005). Large
686 uncertainties also present in the Tethys/Paratethys configuration. The Tethyan Seaway is open
687 with a depth of over 3000 m in F18, in contrast to geological evidence suggesting intermittent
688 openings during ~15-12.8 Ma (Sun et al., 2021). The Paratethys was intermittently connected

a supprimé: Concerning

a mis en forme : Normal (Web)

a supprimé: section

a supprimé: reflects the feature of early to middle Miocene geography, in which the Tethyan Seaway is open, and the size of the IP is small. In the mid-late Miocene, given the final closure of the Tethyan Seaway ~14 Ma (Sun et al., 2021) and remarkable expansion of the Antarctic ice sheets from ~14.2 to 13.8 Ma (Frigola et al., 2018) leading to global sea-level change, the physiography in the Middle East and East Africa, a critical region for SASM development, is much different. As a result, the atmospheric and oceanic circulations are also changed in this region and far end (Hamon et al., 2013).

701 and disconnected from the global ocean during the Middle Miocene according to geological
 702 studies (Rögl, 1997). It is assigned to connect to the global ocean in F18 and Herold et al.
 703 (2008) while it retreats to the Carpathian-Black Sea-Caspian Sea region and is connected with
 704 the Mediterranean in He et al. (2021). In short, the Tethys/Paratethys configuration in F18
 705 reflects more the feature of early Middle Miocene geography, with an open Tethyan Seaway
 706 and a smaller IP. However, given that most reconstruction records focus on the late Middle
 707 Miocene period (14-12 Ma), our Middle Miocene simulations may not adequately capture the
 708 IP's effects and may be less suitable for comparison with proxy data. Nonetheless, a previous
 709 study (Sarr et al., 2022) utilizing a late Miocene (10 Ma) configuration also emphasized the
 710 significant role of the Anatolia–Iran uplift on enhanced SASM. Their experiments showed that
 711 this uplift deepened the low-pressure area over the Arabian Peninsula, intensifying low-level
 712 wind and moisture transport from the Arabian Sea towards South Asia, a process consistent
 713 with our simulations (Fig. 4a). We thus emphasize that constraining the exact timing of IP uplift
 714 is crucial to improve our understanding of the evolution of the SAM. During the late Middle
 715 Miocene period, significant geological events occurred, including the final closure of the
 716 Tethyan Seaway ~14 Ma (Sun et al., 2021) and the remarkable expansion of the Antarctic ice
 717 sheets from ~14.2 to 13.8 Ma (Holbourn et al., 2005), resulting in global sea-level changes.
 718 These geological events likely led to considerable changes in the physiography of the Middle
 719 East and East Africa. Consequently, the atmospheric and oceanic circulations in these regions
 720 and beyond are likely altered during the late Middle Miocene (Hamon et al., 2013). But some
 721 modelling studies indicated that “the sole effect of the Tethys way closure, without strong
 722 modification of land extension in the Arabian Peninsula region, remain limited” (Tardif et al.,
 723 2023), thereby not supporting the hypothesis that the closure of the Tethys Seaway may
 724 contribute to altering the intensity of the monsoon during the Miocene (Bialik et al., 2020; Sun
 725 et al., 2021).

726 The uncertainty regarding the effects of CO₂ on SASM primarily arises from the wide
 727 range of estimated CO₂ values during the Middle Miocene. While our CO₂ sensitivity
 728 experiments cover various concentrations, prior studies (Thomson et al., 2021) indicate that the
 729 impacts of CO₂ variation on SASM are influenced by the background state. For instance, the
 730 status of the Tethys Sea, whether open or closed, introduces uncertain changes in SASM rainfall.
 731 Consequently, understanding the precise impacts of CO₂ variation on SASM behavior remains
 732 complex and warrants further investigation. In brief, the evolution of the SASM during the
 733 Middle Miocene could have been caused by a combination of changes in topography in East

a supprimé: in contrast to

a supprimé: Therefore, it is necessary in our future work to take into account

a supprimé: the effect

a supprimé: the paleogeography change, in particular

a supprimé: closure

a supprimé: Seaway plus the development of the Anatolian Iranian Plateau. The

a supprimé: , geography, the ocean-atmospheric circulation related to decreasing atmospheric CO₂, changes

a supprimé: orbital forcing,

745 African and Middle Eastern physiography, CO₂ variation, as well as the progressive cryosphere
746 expansion in Antarctica. All these factors should be addressed in future study with careful
747 experimental design.

a supprimé: on

a supprimé:

748 High-resolution model is essential to capturing the monsoon dynamics and
749 thermodynamics thus improves our understanding of the monsoonal variation/change (Acosta
750 and Huber, 2017; Anand et al., 2018; Botsyun et al., 2022a, b). The climate model employed in
751 present study is a version of low spatial resolution, not sufficient to reproduce the regional
752 features of the SASM. For instance, the Indo-Gangetic low-level jet, a key mechanism that
753 introduces monsoon onshore flow from the Bay of Bangla into northern India (Acosta and
754 Huber, 2017), is missing in our modern simulation as all the low-resolution models do.
755 Misrepresentation of this circulation is problematic for interpreting the effect of HM uplift and
756 reconciling the modeling-proxy data discrepancy (Khan et al., 2014; Vogeli et al., 2017; Bhatia
757 et al., 2021). The low resolution also likely underestimates the barrier effect of the IP due to
758 topography smooth (Boos and Hurley, 2013). For instance, the mechanical blocking effect is
759 more prominent in the studies with high-resolution models (Tang et al., 2013; Acosta and Huber,
760 2020) than those with coarse resolution model (Zhang et al., 2015; Wu et al., 2007). Although
761 it is out of computer resources to run coupled paleoclimate simulations and perform many
762 sensitivity experiments with high resolution version, we acknowledge that a better
763 understanding of the impact of topographic change on the SASM and the underlying
764 mechanism would benefit from additional simulations performed with increased spatial
765 resolution.

a mis en forme : Couleur de police : Automatique

a supprimé: 2017

a mis en forme : Couleur de police : Automatique

766 The evolution of the SASM is also largely determined by large scale circulation (Wu et.
767 al., 2012; Botsyun et al., 2022b). For instance, the mid-latitude westerly Jet migrated earlier (in
768 the year) and reached higher latitude during warm climate periods than in the pre-industry
769 (Botsyun et al., 2022b). Our Miocene experiments likely confirm this point (not shown) but
770 investigation in depth needs to be done in the future. We also acknowledge that running
771 OAGCMs necessitates an extended period to achieve equilibrium. Particularly with significant
772 modifications to topography or CO₂ levels, integrations spanning 200/500 years may carry the
773 risk of non-equilibrium, potentially affecting the quantitative estimation of their effects, but not
774 essentially change the results.

778 **6. Conclusions**

779 In this study, we performed a series of 12 experiments with the fully coupled OAGCM
780 CESM1.2 (with ~2° horizontal resolution) to investigate the SASM in response to topographic
781 changes in the region surrounding the Tibetan Plateau and the variations of global CO₂
782 concentration during the Middle Miocene. We examined the effect of elevated IP and HM on
783 the SASM through a set of topographic sensitivity experiments. Additionally, due to the large
784 uncertainties of CO₂ reconstructions (Rae et al., 2021; CenCO₂PIP, 2023), we conducted a
785 series of CO₂ sensitivity experiments to investigate its impact on the SASM. We explored the
786 underlying mechanisms and compare the modeling results with proxy data. The conclusions
787 are as follows:

788 (1) We confirm and extend previous studies showing that IP uplift plays a major role in
789 the intensification of the SASM, particularly in the western region, from the northern Arabian
790 Sea to northwestern India and Pakistan, while it has little impact on eastern India. The effect of
791 the HM uplift is confined to the range of the HM and its vicinity, producing orographic
792 precipitation change.

793 (2) The response of the SASM to CO₂ variation under Middle Miocene boundary
794 conditions is similar to that under present-day conditions projecting future SASM changes. This
795 suggests that similar physical processes operate during these two warm periods. Enhanced
796 monsoonal precipitation is primarily governed by enhanced thermodynamic conditions due to
797 atmospheric warming, while the contribution from the change in large-scale monsoon
798 circulation plays a secondary role. In the western region, topographic change, particular the IP
799 uplift, remain the dominant factor.

800 (3) Topographic changes out-compete CO₂ variations in driving the intensification of the
801 SASM. The forcing of CO₂ variation is more important for the change of large-scale monsoon
802 circulation that is decoupled with rainfall change. In case of strong CO₂ variation, that is, from
803 280 to 1000 ppm, similar to the abrupt-3x or 4x CO₂ experiments, its contribution to SASM
804 precipitation is comparable (approximately 75%~100%) to that of topographic forcing in the
805 core SAM region. However, in the western region, topographic forcing remains the dominant
806 factor.

807 (4) We propose a thermodynamic process linking the uplift of the IP to enhanced SASM,
808 where a deepened thermal low transports moisture from the Arabian Sea to the western region,
809 coupled with the South Asian High linked by latent heat release. However, the strong thermal
810 effect of the uplifted IP in our Middle Miocene simulation is possibly associated with the

- a supprimé: perform...erformed a series of 12 experiments with the fully couple...oupled OAGCM CESM1.2 (at...ith ~2° horizontal resolution) to investigate how...the SASM in response to topographic changes in the region surrounding the Tibetan Plateau and the variation...ariations of global CO₂ concentration during the Middle Miocene. On the one hand, we examine...e examined the effect of elevated IP and HM on the SASM with...through a set of topographic sensitivity experiments. On the other hand...dditionally, due t (... [9]
- a supprimé: the
- a mis en forme (... [10]
- a mis en forme : Couleur de police : Automatique
- a supprimé: i.e.,
- a mis en forme : Couleur de police : Automatique
- a supprimé: whereas
- a mis en forme : Couleur de police : Automatique
- a supprimé: in
- a mis en forme : Couleur de police : Automatique
- a supprimé: the
- a mis en forme : Couleur de police : Automatique
- a supprimé: SASM
- a mis en forme (... [11]
- a supprimé: pCO₂
- a mis en forme : Couleur de police : Automatique
- a mis en forme : Couleur de police : Automatique
- a supprimé: in
- a mis en forme (... [12]
- a supprimé: change, suggesting
- a mis en forme : Couleur de police : Automatique
- a supprimé: process operating in the
- a mis en forme : Couleur de police : Automatique
- a supprimé: The enhanced
- a mis en forme : Couleur de police : Automatique
- a supprimé: part
- a mis en forme : Couleur de police : Automatique
- a supprimé: still plays a
- a mis en forme : Couleur de police : Automatique
- a supprimé: role
- a mis en forme : Couleur de police : Automatique
- a supprimé: change...hanges out-competes (... [13]
- a mis en forme : Couleur de police : Automatique
- a supprimé: variation
- a mis en forme : Couleur de police : Automatique
- a supprimé: the
- a mis en forme : Couleur de police : Automatique
- a supprimé: 3x
- a mis en forme (... [14]
- a supprimé: 4x
- a mis en forme : Couleur de police : Automatique
- a supprimé: experiment)...xperiments, its contribution to (... [15]
- a supprimé: A thermodynamical...e propose a thermodyn (... [16]

910 smaller size of the IP and model's low-resolution, which tends to underestimate the mechanical
911 effects.

912 (5) Compared with reconstructions, the effect of IP uplift is in good agreement with
913 observed evolution of precipitation and the change of wind intensity while the effects of the
914 HM uplift and CO₂ variation are insufficient to interpret the proxies.

916 **Author contribution**

917 MZ and YZ wrote the draft manuscript and analyzed the simulations. YS performed the
918 simulations; GR and TZ modified the draft and particularly corrected the abstract and
919 conclusions. YZ and DL conceived and developed the research. All authors participated in the
920 final version of the manuscript.

922 **Competing interest**

923 The authors declare that they have no conflict of interest.

924 **Acknowledgements**

925 This work is jointly supported by the National Natural Science Foundation of China (Grants
926 41988101, 42105047) and the Second Tibetan Plateau Scientific Expedition and Research
927 Program (STEP; Grant No. 2019QZKK0708). Model simulations presented in this study were
928 performed on the supercomputer of Chinese Academy of Science Jin Cloud.

929 **References**

- 930 Acosta, R. P., and M. Huber, 2017: The neglected Indo-Gangetic plains low-level jet and its
931 importance for moisture transport and precipitation during the peak summer monsoon.
932 Geophysical Research Letters, 44, 8601-8610, <https://doi.org/10.1002/2017gl074440>.
- 933 Acosta, R.P., Huber, M., 2020. Competing Topographic Mechanisms for the Summer Indo-
934 Asian Monsoon. Geophysical Research Letters 47, e2019GL085112.
935 <https://doi.org/10.1029/2019GL085112>
- 936 Agard, P., Omrani, J., Jolivet, L., Whitechurch, H., Vrielynck, B., Spakman, W., Monié, P.,
937 Meyer, B., Wortel, R., 2011. Zagros orogeny: a subduction-dominated process.
938 Geological Magazine 148, 692–725. <https://doi.org/10.1017/S001675681100046X>
- 939 Ali, S., E. C. Hathorne, and M. Frank, 2021: Persistent provenance of south asian monsoon-
940 induced silicate weathering over the past 27 million years. Paleoceanography and
941 Paleoclimatology, 36, <https://doi.org/10.1029/2020pa003909>.
- 942 Anand, A., Mishra, S.K., Sahany, S., Bhowmick, M., Rawat, J.S., Dash, S.K., 2018. Indian
943 Summer Monsoon Simulations: Usefulness of Increasing Horizontal Resolution, Manual
944 Tuning, and Semi-Automatic Tuning in Reducing Present-Day Model Biases. Sci Rep 8,
945 3522. <https://doi.org/10.1038/s41598-018-21865-1>

a supprimé: as well as

a supprimé: that

a supprimé: effect

a mis en forme : Couleur de police : Automatique

a supprimé: pCO₂

a mis en forme : Couleur de police : Automatique

a supprimé: inadequate

a mis en forme : Couleur de police : Automatique

a mis en forme : Couleur de police : Automatique

a mis en forme : Couleur de police : Automatique

a mis en forme : Couleur de police : Automatique

a mis en forme : Couleur de police : Automatique

a mis en forme : Couleur de police : Automatique

951 An, Z. S., J. E. Kutzbach, W. L. Prell, and S. C. Porter, 2001: Evolution of asian monsoons and
952 phased uplift of the himalayan tibetan plateau since late miocene times. *Nature*, 411, 62-
953 66, <https://doi.org/10.1038/35075035>.

954 Ballato, P., Cifelli, F., Heidarzadeh, G., Ghassemi, M.R., Wickert, A.D., Hassanzadeh, J.,
955 Dupont-Nivet, G., Balling, P., Sudo, M., Zeilinger, G., Schmitt, A.K., Mattei, M., Strecker,
956 M.R., 2017. Tectono-sedimentary evolution of the northern Iranian Plateau: insights from
957 middle-late Miocene foreland-basin deposits. *Basin Research* 29, 417–446.
958 <https://doi.org/10.1111/bre.12180>

959 Betzler, C., and Coauthors, 2016: The abrupt onset of the modern south asian monsoon winds.
960 *Sci. Rep.*, 6, <https://doi.org/10.1038/srep29838>.

961 Bhatia, H., Srivastava, G., Spicer, R.A., Farnsworth, A., Spicer, T.E.V., Mehrotra, R.C.,
962 Paudyal, K.N., Valdes, P., 2021. Leaf physiognomy records the Miocene intensification
963 of the South Asia Monsoon. *Global and Planetary Change* 196, 103365.
964 <https://doi.org/10.1016/j.gloplacha.2020.103365>

965 Bialik, O. M., G. Auer, N. O. Ogawa, D. Kroon, N. D. Waldmann, and N. Ohkouchi, 2020:
966 Monsoons, upwelling, and the deoxygenation of the northwestern indian ocean in response
967 to middle to late miocene global climatic shifts. *Paleoceanography and Paleoclimatology*,
968 35, <https://doi.org/10.1029/2019pa003762>.

969 Boos, W., Kuang, Z., 2010. Dominant control of the South Asian Monsoon by orographic
970 insulation versus plateau heating. *Nature* 463, 218–22.
971 <https://doi.org/10.1038/nature08707>

972 Boos, W.R., Hurley, J.V., 2013. Thermodynamic Bias in the Multimodel Mean Boreal Summer
973 Monsoon. *Journal of Climate* 26, 2279–2287. <https://doi.org/10.1175/JCLI-D-12-00493.1>

974 Botsyun, S., Ehlers, T.A., Koptev, A., Böhme, M., Methner, K., Risi, C., Stepanek, C., Mutz,
975 S.G., Werner, M., Boateng, D., Mulch, A., 2022a. Middle Miocene Climate and Stable
976 Oxygen Isotopes in Europe Based on Numerical Modeling. *Paleoceanography and*
977 *Paleoclimatology* 37, e2022PA004442. <https://doi.org/10.1029/2022PA004442>

978 Botsyun, S., Mutz, S.G., Ehlers, T.A., Koptev, A., Wang, X., Schmidt, B., Appel, E., Scherer,
979 D.E., 2022b. Influence of Large-Scale Atmospheric Dynamics on Precipitation
980 Seasonality of the Tibetan Plateau and Central Asia in Cold and Warm Climates During
981 the Late Cenozoic. *Journal of Geophysical Research: Atmospheres* 127, e2021JD035810.
982 <https://doi.org/10.1029/2021JD035810>

983 Burls, N.J., Bradshaw, C.D., Boer, A.M.D., Herold, N., Huber, M., Pound, M., Donnadieu, Y.,
984 Farnsworth, A., Frigola, A., Gasson, E., Heydt, A.S. von der, Hutchinson, D.K., Knorr, G.,
985 Lawrence, K.T., Lear, C.H., Li, X., Lohmann, G., Lunt, D.J., Marzocchi, A., Prange, M.,
986 Riihimaki, C.A., Sarr, A.-C., Siler, N., Zhang, Z., 2021. Simulating Miocene Warmth:
987 Insights From an Opportunistic Multi-Model Ensemble (MioMIP1). *Paleoceanography*
988 *and Paleoclimatology* 36, e2020PA004054. <https://doi.org/10.1029/2020PA004054>

989 Chakraborty, A., Nanjundiah, R.S., Srinivasan, J., 2006. Theoretical aspects of the onset of
990 Indian summer monsoon from perturbed orography simulations in a GCM. *Annales*
991 *Geophysicae* 24, 2075–2089.

992 Chen, G.-S., Liu, Z., Kutzbach, J., 2014. Reexamining the barrier effect of the Tibetan Plateau
993 on the South Asian summer monsoon. *Climate of the Past* 10. <https://doi.org/10.5194/cp-10-1269-2014>

994
995 Chou, C., J. D. Neelin, C.-A. Chen, and J.-Y. Tu, 2009: Evaluating the "rich-get-richer"
996 mechanism in tropical precipitation change under global warming. *J. Climate*, 22, 1982-
997 2005, <https://doi.org/10.1175/2008jcli2471.1>.

998 Clift, P.D., Hodges, K.V., Heslop, D., Hannigan, R., Van Long, H., Calves, G., 2008.
999 Correlation of Himalayan exhumation rates and Asian monsoon intensity. *Nature Geosci*
1000 1, 875–880. <https://doi.org/10.1038/ngeo351>

1001 Clift, P.D., Webb, A.A.G., 2019. A history of the Asian monsoon and its interactions with solid
1002 Earth tectonics in Cenozoic South Asia. Geological Society, London, Special Publications
1003 483, 631–652. <https://doi.org/10.1144/SP483.1>

1004 Ding, L., Spicer, R.A., Yang, J., Xu, Q., Cai, F., Li, S., Lai, Q., Wang, H., Spicer, T.E.V., Yue,
1005 Y., Shukla, A., Srivastava, G., Khan, M.A., Bera, S., Mehrotra, R., 2017. Quantifying the
1006 rise of the Himalaya orogen and implications for the South Asian monsoon. *Geology* 45,
1007 215–218. <https://doi.org/10.1130/G38583.1>

1008 Ding, L., P. Kapp, F. Cai, C. N. Garzzone, Z. Xiong, H. Wang, and C. Wang, 2022: Timing and
1009 mechanisms of tibetan plateau uplift. *Nature Reviews Earth & Environment*,
1010 <https://doi.org/10.1038/s43017-022-00318-4>.

1011 Endo, H., and A. Kitoh, 2014: Thermodynamic and dynamic effects on regional monsoon
1012 rainfall changes in a warmer climate. *Geophysical Research Letters*, 41, 1704-1710,
1013 <https://doi.org/10.1002/2013gl059158>.

1014 Eyring, V., Bony, S., Meehl, G.A., Senior, C.A., Stevens, B., Stouffer, R.J., Taylor, K.E., 2016.
1015 Overview of the Coupled Model Intercomparison Project Phase 6 (CMIP6) experimental
1016 design and organization. *Geoscientific Model Development* 9, 1937–1958.
1017 <https://doi.org/10.5194/gmd-9-1937-2016>

1018 Farnsworth, A., Lunt, D.J., Robinson, S.A., Valdes, P.J., Roberts, W.H.G., Clift, P.D.,
1019 Markwick, P., Su, T., Wrobel, N., Bragg, F., Kelland, S.-J., Pancost, R.D., 2019. Past East
1020 Asian monsoon evolution controlled by paleogeography, not CO₂. *Science Advances* 5,
1021 eaax1697. <https://doi.org/10.1126/sciadv.aax1697>

1022 Fluteau, F., Ramstein, G., Besse, J., 1999. Simulating the evolution of the Asian and African
1023 monsoons during the past 30 Myr using an atmospheric general circulation model. *Journal*
1024 *of Geophysical Research: Atmospheres* 104, 11995–12018.
1025 <https://doi.org/10.1029/1999JD900048>

1026 Frigola, A., Prange, M., Schulz, M., 2018. Boundary conditions for the Middle Miocene
1027 Climate Transition (MMCT v1. 0). *Geoscientific Model Development* 11, 1607–1626.

1028 Gent, P.R., Danabasoglu, G., Donner, L.J., Holland, M.M., Hunke, E.C., Jayne, S.R., Lawrence,
1029 D.M., Neale, R.B., Rasch, P.J., Vertenstein, M., Worley, P.H., Yang, Z.-L., Zhang, M.,
1030 2011. The Community Climate System Model Version 4. *Journal of Climate* 24, 4973–
1031 4991. <https://doi.org/10.1175/2011JCLI4083.1>

1032 Goldner, A., Herold, N., Huber, M., 2014. The Challenge of Simulating the Warmth of the Mid-
1033 Miocene Climatic Optimum in CESM1. *Climate of the Past*.

1034 Gupta, A. K., A. Yuvaraja, M. Prakasam, S. C. Clemens, and A. Velu, 2015: Evolution of the
1035 south asian monsoon wind system since the late middle miocene. *Palaeogeography*
1036 *Palaeoclimatology Palaeoecology*, 438, 160-167,
1037 <https://doi.org/10.1016/j.palaeo.2015.08.006>.

1038 Hamon, N., Sepulchre, P., Lefebvre, V., Ramstein, G., 2013. The role of eastern Tethys seaway
1039 closure in the Middle Miocene Climatic Transition (ca. 14 Ma). *Climate of the Past* 9,
1040 2687–2702. <https://doi.org/10.5194/cp-9-2687-2013>

1041 Harris, N., 2006. The elevation history of the Tibetan Plateau and its implications for the Asian
1042 monsoon. *Palaeogeography, Palaeoclimatology, Palaeoecology, Monsoon and Tectonics*
1043 *of Asia* 241, 4–15. <https://doi.org/10.1016/j.palaeo.2006.07.009>

1044 He, B., 2017. Influences of elevated heating effect by the Himalaya on the changes in Asian
1045 summer monsoon. *Theor Appl Climatol* 128, 905–917. [https://doi.org/10.1007/s00704-](https://doi.org/10.1007/s00704-016-1746-5)
1046 [016-1746-5](https://doi.org/10.1007/s00704-016-1746-5)

1047 [He, Z., Zhang, Z., Guo, Z., Scotese, C.R., Deng, C., 2021. Middle Miocene \(~14 Ma\) and Late](https://doi.org/10.1029/2021PA004298)
1048 [Miocene \(~6 Ma\) Paleogeographic Boundary Conditions. *Paleoceanography and*](https://doi.org/10.1029/2021PA004298)
1049 [*Palaeoclimatology* 36, e2021PA004298. <https://doi.org/10.1029/2021PA004298>](https://doi.org/10.1029/2021PA004298)

1050 Herold, N., M. Huber, and R. D. Mueller, 2011: Modeling the miocene climatic optimum. Part

1051 i: Land and atmosphere. *J. Climate*, 24, 6353-6372, <https://doi.org/10.1175/2011jcli4035.1>.
 1052 [Herold, N., Seton, M., Müller, R.D., You, Y., Huber, M., 2008. Middle Miocene tectonic](#)
 1053 [boundary conditions for use in climate models. *Geochemistry, Geophysics,*](#)
 1054 [Geosystems 9.](#)
 1055 Hersbach, H., and Coauthors, 2020: The era5 global reanalysis. *Quarterly Journal of the Royal*
 1056 *Meteorological Society*, 146, 1999-2049, <https://doi.org/10.1002/qj.3803>.
 1057 [Holbourn, A., Kuhnt, W., Schulz, M., Erlenkeuser, H., 2005. Impacts of orbital forcing and](#)
 1058 [atmospheric carbon dioxide on Miocene ice-sheet expansion. *Nature* 438, 483–487.](#)
 1059 <https://doi.org/10.1038/nature04123>
 1060 Huffman, G. J., R. F. Adler, D. T. Bolvin, and G. Gu, 2009: Improving the global precipitation
 1061 record: Gcp version 2.1. *Geophys. Res. Lett.*, 36, <https://doi.org/10.1029/2009gl040000>.
 1062 Hunke, E.C., Lipscomb, W.H., 2010. CICE: the Los Alamos Sea Ice Model Documentation
 1063 and Software User’s Manual Version 4. 1–76.
 1064 Jin, C., B. Wang, and J. Liu, 2020: Future changes and controlling factors of the eight regional
 1065 monsoons projected by cmip6 models. *J. Climate*, 33, 9307-9326,
 1066 <https://doi.org/10.1175/jcli-d-20-0236.1>.
 1067 Khan, M.A., Spicer, R.A., Bera, S., Ghosh, R., Yang, J., Spicer, T.E.V., Guo, S., Su, T., Jacques,
 1068 F., Grote, P.J., 2014. Miocene to Pleistocene floras and climate of the Eastern Himalayan
 1069 Siwaliks, and new palaeoelevation estimates for the Namling–Oiyug Basin, Tibet. *Global*
 1070 *and Planetary Change* 113, 1–10. <https://doi.org/10.1016/j.gloplacha.2013.12.003>
 1071 Kitoh, A., 2002. Effects of Large-Scale Mountains on Surface Climate. A Coupled Ocean-
 1072 Atmosphere General Circulation Model Study. *Journal of the Meteorological Society of*
 1073 *Japan* 80, 1165–1181. <https://doi.org/10.2151/jmsj.80.1165>
 1074 Kong, Y., Y. Wu, X. Hu, Y. Li, and S. Yang, 2022: Uncertainty in projections of the south
 1075 Asian summer monsoon under global warming by cmip6 models: Role of tropospheric
 1076 meridional thermal contrast. *Atmospheric and Oceanic Science Letters*, 15, 100145,
 1077 <https://doi.org/https://doi.org/10.1016/j.aosl.2021.100145>.
 1078 Krapp, M., and J. H. Jungclauss, 2011: The middle miocene climate as modelled in an
 1079 atmosphere-ocean-biosphere model. *Climate Past*, 7, 1169-1188,
 1080 <https://doi.org/10.5194/cp-7-1169-2011>.
 1081 Kutzbach, J.E., Guetter, P.J., Ruddiman, W.F., Prell, W.L., 1989. Sensitivity of climate to late
 1082 Cenozoic uplift in southern Asia and the American west: Numerical experiments. *Journal*
 1083 *of Geophysical Research: Atmospheres* 94, 18393–18407.
 1084 <https://doi.org/10.1029/JD094iD15p18393>
 1085 Lawrence, D.M., Oleson, K.W., Flanner, M.G., Thornton, P.E., Swenson, S.C., Lawrence, P.J.,
 1086 Zeng, X., Yang, Z.-L., Levis, S., Sakaguchi, K., Bonan, G.B., Slater, A.G., 2011.
 1087 Parameterization improvements and functional and structural advances in Version 4 of the
 1088 Community Land Model. *Journal of Advances in Modeling Earth Systems* 3, M03001.
 1089 <https://doi.org/10.1029/2011MS00045>
 1090 Licht, A., and Coauthors, 2014: Asian monsoons in a late eocene greenhouse world. *Nature*,
 1091 513, 501-506, <https://doi.org/10.1038/nature13704>.
 1092 Liu, X., and B. Dong, 2013: Influence of the tibetan plateau uplift on the asian monsoon-arid
 1093 environment evolution. *Chinese Science Bulletin*, 58, 4277-4291,
 1094 <https://doi.org/10.1007/s11434-013-5987-8>.
 1095 Liu, X., Xu, Q., Ding, L., 2016. Differential surface uplift: Cenozoic paleoelevation history of
 1096 the Tibetan Plateau. *Sci. China Earth Sci.* 59, 2105–2120. [https://doi.org/10.1007/s11430-](https://doi.org/10.1007/s11430-015-5486-y)
 1097 [015-5486-y](https://doi.org/10.1007/s11430-015-5486-y)
 1098 Liu, Y., Wang, Z., Zhuo, H., Wu, G., 2017. Two types of summertime heating over Asian large-
 1099 scale orography and excitation of potential-vorticity forcing II. Sensible heating over
 1100 Tibetan-Iranian Plateau. *Sci. China Earth Sci.* 60, 733–744.

1101 <https://doi.org/10.1007/s11430-016-9016-3>

1102 Manabe, S., Terpstra, T.B., 1974. The Effects of Mountains on the General Circulation of the
1103 Atmosphere as Identified by Numerical Experiments. *Journal of the Atmospheric Sciences*
1104 31, 3–42. [https://doi.org/10.1175/1520-0469\(1974\)031<0003:TEOMOT>2.0.CO;2](https://doi.org/10.1175/1520-0469(1974)031<0003:TEOMOT>2.0.CO;2)

1105 [Macgregor, D., 2015: History of the development of the east african rift system: A series of](#)
1106 [interpreted maps through time. *Journal of African Earth Sciences*, 101, 232-252,](#)
1107 <https://doi.org/10.1016/j.jafrearsci.2014.09.016>.

1108 McQuarrie, N., Stock, J.M., Verdel, C., Wernicke, B.P., 2003. Cenozoic evolution of Neotethys
1109 and implications for the causes of plate motions. *Geophysical Research Letters* 30.
1110 <https://doi.org/10.1029/2003GL017992>

1111 [Medina, S., Houze Jr., R.A., Kumar, A., Niyogi, D., 2010. Summer monsoon convection in the](#)
1112 [Himalayan region: terrain and land cover effects. *Quarterly Journal of the Royal*](#)
1113 [Meteorological Society](#) 136, 593–616. <https://doi.org/10.1002/qj.601>

1114 [Miao, Y., Fang, X., Sun, J., Xiao, W., Yang, Y., Wang, X., Farnsworth, A., Huang, K., Ren,](#)
1115 [Y., Wu, F., Qiao, Q., Zhang, W., Meng, Q., Yan, X., Zheng, Z., Song, C., Utescher, T.,](#)
1116 [2022. A new biologic paleoaltimetry indicating Late Miocene rapid uplift of northern Tibet](#)
1117 [Plateau. *Science* 378, 1074–1079. <https://doi.org/10.1126/science.abo2475>](#)

1118 Mouthereau, F., 2011. Timing of uplift in the Zagros belt/Iranian plateau and accommodation
1119 of late Cenozoic Arabia–Eurasia convergence. *Geological Magazine* 148, 726–738.
1120 <https://doi.org/10.1017/S0016756811000306>

1121 Neale, R.B., Richter, J., Park, S., Lauritzen, P.H., Vavrus, S.J., Rasch, P.J., Zhang, M., 2013.
1122 The Mean Climate of the Community Atmosphere Model (CAM4) in Forced SST and
1123 Fully Coupled Experiments. *Journal of Climate* 26, 5150–5168.
1124 <https://doi.org/10.1175/JCLI-D-12-00236.1>

1125 Prell, W. L., and J. E. Kutzbach, 1992: Sensitivity of the indian monsoon to forcing parameters
1126 and implications for its evolution. *Nature*, 360, 647-652, <https://doi.org/10.1038/360647a0>.

1127 Ramstein, G., Fluteau, F., Besse, J., Joussaume, S., 1997. Effect of orogeny, plate motion and
1128 land-sea distribution on Eurasian climate change over the past 30 million years. Effect of
1129 orogeny, plate motion and land-sea distribution on Eurasian climate change over the past
1130 30 million years 386, 788–795.

1131 Reuter, M., W. E. Piller, M. Harzhauser, and A. Kroh, 2013: Cyclone trends constrain monsoon
1132 variability during late oligocene sea level highstands (kachchh basin, nw india). *Climate*
1133 *Past*, 9, 2101-2115, <https://doi.org/10.5194/cp-9-2101-2013>.

1134 [Rögl, F., 1997. Palaeogeographic Considerations for Mediterranean and Paratethys Seaways](#)
1135 [\(Oligocene to Miocene\). *Annalen des Naturhistorischen Museums in Wien. Serie A für*](#)
1136 [Mineralogie und Petrographie, Geologie und Paläontologie, Anthropologie und](#)
1137 [Prähistorie](#) 99, 279–310.

1138 Sarr, A.-C., and Coauthors, 2022: Neogene south asian monsoon rainfall and wind histories
1139 diverged due to topographic effects. *Nat Geosci*, 15, 314+,
1140 <https://doi.org/10.1038/s41561-022-00919-0>.

1141 Smith, R., P. Jones, B. Briegleb, F. Bryan, and S. Yeager, 2010: The parallel ocean program
1142 (pop) reference manual: Ocean component of the community climate system model (ccsm).

1143 Steinthorsdottir, M., Coxall, H., De Boer, A., Huber, M., Barbolini, N., Bradshaw, C., Burls,
1144 N., Feakins, S., Gasson, E., Henderiks, J., Holbourn, A.E., Kiel, S., Kohn, M., Knorr, G.,
1145 Kürschner, W.M., Lear, C.H., Liebrand, D., Lunt, D.J., Mörs, T., Pearson, P., Pound, M.J.,
1146 Stoll, H., Stromberg, C., 2021. The Miocene: The Future of the Past. *Paleoceanography*
1147 *and Paleoclimatology* 36. <https://doi.org/10.1029/2020PA004037>

1148 [Stoker, M.S., Praeg, D., Hjelstuen, B.O., Laberg, J.S., Nielsen, T., Shannon, P.M., 2005.](#)
1149 [Neogene stratigraphy and the sedimentary and oceanographic development of the NW](#)

- 1150 [European Atlantic margin. *Marine and Petroleum Geology*, The STRATAGEM Project](#)
 1151 [22, 977–1005. <https://doi.org/10.1016/j.marpetgeo.2004.11.007>](#)
- 1152 Su, B., Jiang, D., Zhang, R., Sepulchre, P., Ramstein, G., 2018. Difference between the North
 1153 Atlantic and Pacific meridional overturning circulation in response to the uplift of the
 1154 Tibetan Plateau. *Climate of the Past* 14, 751–762. <https://doi.org/10.5194/cp-14-751-2018>
- 1155 Sun, J., Sheykh, M., Ahmadi, N., Cao, M., Zhang, Z., Tian, S., Sha, J., Jian, Z., Windley, B.F.,
 1156 Talebian, M., 2021. Permanent closure of the Tethyan Seaway in the northwestern Iranian
 1157 Plateau driven by cyclic sea-level fluctuations in the late Middle Miocene.
 1158 *Palaeogeography, Palaeoclimatology, Palaeoecology* 564, 110172.
 1159 <https://doi.org/10.1016/j.palaeo.2020.110172>
- 1160 Sun, Y., and Coauthors, 2023: Revisiting the physical mechanisms of east Asian summer
 1161 monsoon precipitation changes during the mid-Holocene: A data–model comparison.
 1162 *Climate Dynamics*, 60, 1009-1022, <https://doi.org/10.1007/s00382-022-06359-1>.
- 1163 Tada, R., H. Zheng, and P. D. Clift, 2016: Evolution and variability of the asian monsoon and
 1164 its potential linkage with uplift of the himalaya and tibetan plateau. *Progress in Earth and*
 1165 *Planetary Science*, 3, <https://doi.org/10.1186/s40645-016-0080-y>.
- 1166 [Tan, M., Zhu, X., Liu, Q., Zhang, Z., Liu, W., 2020. Multiple fluvial styles in Late Miocene](#)
 1167 [post-rift successions of the offshore Bohai Bay Basin \(China\): Evidence from a seismic](#)
 1168 [geomorphological study. *Marine and Petroleum Geology* 113, 104173.](#)
 1169 <https://doi.org/10.1016/j.marpetgeo.2019.104173>
- 1170 Tang, H., Micheels, A., Eronen, J.T., Ahrens, B., Fortelius, M., 2013. Asynchronous responses
 1171 of East Asian and Indian summer monsoons to mountain uplift shown by regional climate
 1172 modelling experiments. *Clim Dyn* 40, 1531–1549. [https://doi.org/10.1007/s00382-012-](https://doi.org/10.1007/s00382-012-1603-x)
 1173 [1603-x](https://doi.org/10.1007/s00382-012-1603-x)
- 1174 Tardif, D., Fluteau, F., Donnadieu, Y., Le Hir, G., Ladant, J.-B., Sepulchre, P., Licht, A.,
 1175 Poblete, F., Dupont-Nivet, G., 2020. The origin of Asian monsoons: a modelling
 1176 perspective. *Climate of the Past* 16, 847–865. <https://doi.org/10.5194/cp-16-847-2020>
- 1177 Tardif, D., and Coauthors, 2023: The role of paleogeography in Asian monsoon evolution: A
 1178 review and new insights from climate modelling. *Earth-Science Reviews*, 243, 104464,
 1179 <https://doi.org/https://doi.org/10.1016/j.earscirev.2023.104464>.
- 1180 The Cenozoic, C. O. P. I. P. C., and Coauthors: Toward a Cenozoic history of atmospheric co2.
 1181 *Science*, 382, eadi5177, <https://doi.org/10.1126/science.adi5177>.
- 1182 [Thomson, J. R., P. B. Holden, P. Anand, N. R. Edwards, C. A. Porchier, and N. B. W. Harris.](#)
 1183 [2021: Tectonic and climatic drivers of asian monsoon evolution. *Nat. Commun.*, 12, 4022,](#)
 1184 <https://doi.org/10.1038/s41467-021-24244-z>.
- 1185 Vogeli, N., P. Huyghe, P. van der Beek, Y. Najman, E. Garzanti, and C. Chauvel, 2017:
 1186 Weathering regime in the eastern himalaya since the mid-miocene: Indications from detrital
 1187 geochemistry and clay mineralogy of the kameng river section, arunachal pradesh, india.
 1188 *Basin Research*, 30, 59-74, <https://doi.org/10.1111/bre.12242>.
- 1189 Wang, C., Dai, J., Zhao, X., Li, Y., Graham, S.A., He, D., Ran, B., Meng, J., 2014. Outward-
 1190 growth of the Tibetan Plateau during the Cenozoic: A review. *Tectonophysics* 621, 1–43.
 1191 <https://doi.org/10.1016/j.tecto.2014.01.036>
- 1192 Wang, Z., Duan, A., Yang, S., 2019. Potential regulation on the climatic effect of Tibetan
 1193 Plateau heating by tropical air–sea coupling in regional models. *Clim Dyn* 52, 1685–1694.
 1194 <https://doi.org/10.1007/s00382-018-4218-z>
- 1195 Wu, G., Liu, Y., He, B., Bao, Q., Duan, A., Jin, F.-F., 2012. Thermal Controls on the Asian
 1196 Summer Monsoon. *Scientific Reports* 2, 404. <https://doi.org/10.1038/srep00404>
- 1197 Wu, G., Liu, Y., Zhang, Q., Duan, A., Wang, T., Wan, R., Liu, X., Li, W., Wang, Z., Liang, X.,
 1198 2007. The Influence of Mechanical and Thermal Forcing by the Tibetan Plateau on Asian
 1199 Climate. *Journal of Hydrometeorology* 8, 770–789. <https://doi.org/10.1175/JHM609.1>

1200 Yang, X., Groeneveld, J., Jian, Z., Steinke, S., Giosan, L., 2020. Middle Miocene Intensification
1201 of South Asian Monsoonal Rainfall. *Paleoceanography and Paleoclimatology* 35,
1202 e2020PA003853. <https://doi.org/10.1029/2020PA003853>

1203 Zhang, R., Jiang, D., Liu, X., Tian, Z., 2012. Modeling the climate effects of different
1204 subregional uplifts within the Himalaya-Tibetan Plateau on Asian summer monsoon
1205 evolution. *Chin. Sci. Bull.* 57, 4617–4626. <https://doi.org/10.1007/s11434-012-5284-y>

1206 Zhang, R., Jiang, D., Zhang, Z., 2019. Vegetation and Ocean Feedbacks on the Asian Climate
1207 Response to the Uplift of the Tibetan Plateau. *Journal of Geophysical Research:*
1208 *Atmospheres* 124, 6327–6341. <https://doi.org/10.1029/2019JD030503>

1209 Zhang, R., Jiang, D., Zhang, Z., Yu, E., 2015. The impact of regional uplift of the Tibetan
1210 Plateau on the Asian monsoon climate. *Palaeogeography, Palaeoclimatology,*
1211 *Palaeoecology* 417, 137–150. <https://doi.org/10.1016/j.palaeo.2014.10.030>

1212

1213

a supprimé: Zhuang, G., Pagani, M., Zhang, Y.G., 2017. Monsoonal upwelling in the western Arabian Sea since the middle Miocene. *Geology* 45, 655–658. <https://doi.org/10.1130/G39013.1>

a mis en forme : Couleur de police : Automatique

1225

Table 2. Evidence of modern SAM in middle Miocene from recently published studies.

No	station	Location (lat/lon)	Proxies	Intensification age (Ma)	Trend*	variable	ref
1	Well Indus Marine A-1	24/66	weathering	15~12	decreasing	Precip	Chal. al.
2	ODP 359	5/73	Sedimentary & geochemical record	12.9	increasing	wind	Beal. al.
3	ODP 722B	16.6/59.8	Bio-marker	12.9	increasing	wind	Gu. al.
4	ODP 722B	16.6/59.8	Bio-marker	14	increasing	wind	Bi. al.
4	NGHP-01-01A	15/71	Bio-marker	14	increasing	Precip	Ya. al.
5	Varkala	8.7/76.7	Pollen fossil	17-15	No change	Precip.	Re. al.
6	ODP 758	5.4/90.4	weathering	13.9	increasing	wind	Al. al.
7	Surai Khola	27.8/83	Leaf Fossil	13	increasing	Precip.	Sri. et al., 2020
8	Darjeeling	27/88.5	Leaf Fossil	13	increasing	Precip.	Kh. al., 2014
9	Arunachal Pradesh	27/93.5	Leaf Fossil	13	No change	Precip.	Kh. al., 2014
9	Arunachal Pradesh	26/93.5	weathering	13	No change	Precip.	Vd. al., 2017

* Trend of monsoon index change from middle to late Miocene.

a supprimé: Evidences

a mis en forme : Couleur de police : Automatique

a supprimé: sample

a mis en forme : Couleur de police : Automatique

a mis en forme : Couleur de police : Automatique

a mis en forme : Couleur de police : Automatique

a supprimé: deposit

a mis en forme : Couleur de police : Automatique

a mis en forme : Couleur de police : Automatique

a supprimé: ODP 722B

... [17]

a mis en forme : Couleur de police : Automatique

a supprimé: Precip

a mis en forme : Couleur de police : Automatique

a mis en forme : Couleur de police : Automatique

a mis en forme : Couleur de police : Automatique

a mis en forme : Couleur de police : Automatique

a mis en forme : Couleur de police : Automatique

a mis en forme : Couleur de police : Automatique

a mis en forme : Couleur de police : Automatique

a mis en forme : Couleur de police : Automatique

a mis en forme : Couleur de police : Automatique

a mis en forme : Couleur de police : Automatique

a mis en forme : Couleur de police : Automatique

1226
1227

Page 4 : [1] a mis en forme author 14/05/2024 14:25:00

Couleur de police : Automatique

Page 4 : [1] a mis en forme author 14/05/2024 14:25:00

Couleur de police : Automatique

Page 4 : [1] a mis en forme author 14/05/2024 14:25:00

Couleur de police : Automatique

Page 4 : [2] a mis en forme author 14/05/2024 14:25:00

Couleur de police : Automatique

Page 4 : [2] a mis en forme author 14/05/2024 14:25:00

Couleur de police : Automatique

Page 4 : [3] a mis en forme author 14/05/2024 14:25:00

Couleur de police : Automatique

Page 4 : [3] a mis en forme author 14/05/2024 14:25:00

Couleur de police : Automatique

Page 4 : [3] a mis en forme author 14/05/2024 14:25:00

Couleur de police : Automatique

Page 4 : [3] a mis en forme author 14/05/2024 14:25:00

Couleur de police : Automatique

Page 4 : [4] a supprimé author 14/05/2024 14:25:00

▼.....

Page 4 : [4] a supprimé author 14/05/2024 14:25:00

▼.....

Page 4 : [5] a supprimé author 14/05/2024 14:25:00

▼.....

Page 4 : [5] a supprimé author 14/05/2024 14:25:00

▼.....

Page 4 : [5] a supprimé author 14/05/2024 14:25:00

▼.....

Page 4 : [5] a supprimé author 14/05/2024 14:25:00

▼.....

Page 4 : [6] a mis en forme author 14/05/2024 14:25:00

Couleur de police : Automatique

Page 4 : [6] a mis en forme author 14/05/2024 14:25:00

Couleur de police : Automatique

Page 4 : [7] a mis en forme author 14/05/2024 14:25:00

Couleur de police : Automatique

Page 4 : [7] a mis en forme author 14/05/2024 14:25:00

Couleur de police : Automatique

Page 4 : [8] a mis en forme author 14/05/2024 14:25:00

Couleur de police : Automatique

Page 4 : [8] a mis en forme author 14/05/2024 14:25:00

Couleur de police : Automatique

Page 4 : [8] a mis en forme author 14/05/2024 14:25:00

Couleur de police : Automatique

Page 4 : [8] a mis en forme author 14/05/2024 14:25:00

Couleur de police : Automatique

Page 4 : [8] a mis en forme author 14/05/2024 14:25:00

Couleur de police : Automatique

Page 4 : [8] a mis en forme author 14/05/2024 14:25:00

Couleur de police : Automatique

Page 4 : [8] a mis en forme author 14/05/2024 14:25:00

Couleur de police : Automatique

Page 4 : [8] a mis en forme author 14/05/2024 14:25:00

Couleur de police : Automatique

Page 4 : [8] a mis en forme author 14/05/2024 14:25:00

Couleur de police : Automatique

Page 4 : [8] a mis en forme author 14/05/2024 14:25:00

Couleur de police : Automatique

Page 4 : [8] a mis en forme author 14/05/2024 14:25:00

Couleur de police : Automatique

Page 4 : [8] a mis en forme author 14/05/2024 14:25:00

Couleur de police : Automatique

Page 4 : [8] a mis en forme author 14/05/2024 14:25:00

Couleur de police : Automatique

Page 28 : [9] a supprimé author 14/05/2024 14:25:00

▼

Page 28 : [9] a supprimé author 14/05/2024 14:25:00

▼

Page 28 : [9] a supprimé author 14/05/2024 14:25:00

▼

Page 28 : [9] a supprimé author 14/05/2024 14:25:00

▼

Page 28 : [9] a supprimé author 14/05/2024 14:25:00

▼

Page 28 : [9] a supprimé author 14/05/2024 14:25:00

▼

Page 28 : [9] a supprimé author 14/05/2024 14:25:00

▼

Page 28 : [9] a supprimé author 14/05/2024 14:25:00

Page 28 : [9] a supprimé author 14/05/2024 14:25:00

Page 28 : [9] a supprimé author 14/05/2024 14:25:00

Page 28 : [9] a supprimé author 14/05/2024 14:25:00

Page 28 : [9] a supprimé author 14/05/2024 14:25:00

Page 28 : [10] a mis en forme author 14/05/2024 14:25:00

Couleur de police : Automatique

Page 28 : [10] a mis en forme author 14/05/2024 14:25:00

Couleur de police : Automatique

Page 28 : [11] a mis en forme author 14/05/2024 14:25:00

Couleur de police : Automatique

Page 28 : [11] a mis en forme author 14/05/2024 14:25:00

Couleur de police : Automatique

Page 28 : [12] a mis en forme author 14/05/2024 14:25:00

Couleur de police : Automatique

Page 28 : [12] a mis en forme author 14/05/2024 14:25:00

Couleur de police : Automatique

Page 28 : [13] a supprimé author 14/05/2024 14:25:00

Page 28 : [13] a supprimé author 14/05/2024 14:25:00

Page 28 : [14] a mis en forme author 14/05/2024 14:25:00

Couleur de police : Gris foncé, Français, Motif : Transparente (Blanc)

Page 28 : [15] a supprimé author 14/05/2024 14:25:00

Page 28 : [15] a supprimé author 14/05/2024 14:25:00

Page 28 : [15] a supprimé author 14/05/2024 14:25:00

Page 28 : [15] a supprimé author 14/05/2024 14:25:00

Page 28 : [15] a supprimé author 14/05/2024 14:25:00

▼

Page 28 : [15] a supprimé author 14/05/2024 14:25:00

▼

Page 28 : [16] a supprimé author 14/05/2024 14:25:00

▼

Page 28 : [16] a supprimé author 14/05/2024 14:25:00

▼

Page 28 : [16] a supprimé author 14/05/2024 14:25:00

▼

Page 28 : [16] a supprimé author 14/05/2024 14:25:00

▼

Page 28 : [16] a supprimé author 14/05/2024 14:25:00

▼

Page 28 : [16] a supprimé author 14/05/2024 14:25:00

▼

Page 28 : [16] a supprimé author 14/05/2024 14:25:00

▼

Page 28 : [16] a supprimé author 14/05/2024 14:25:00

▼

Page 37 : [17] a supprimé author 14/05/2024 14:25:00